Proteomic Analysis Uncovers Measles Virus Protein C Interaction With p65–iASPP Protein Complex

Alice Meignié, Chantal Combredet, Marc Santolini, István Kovács, Thibaut Douché, Quentin Giai Gianetto, Hyeju Eun, Mariette I Matondo, Yves Jacob, Regis Grailhe, et al.

HAL Id: **pasteur-03184181**
https://pasteur.hal.science/pasteur-03184181

Submitted on 29 Mar 2021

Proteomic Analysis Uncovers Measles Virus Protein C Interaction With p65–iASPP Protein Complex

Authors

Alice Meignié, Chantal Combredet, Marc Santolini, István A. Kovács, Thibaut Douché, Quentin Giai Gianetto, Hyeju Eun, Mariette Matondo, Yves Jacob, Regis Grailhe, Frédéric Tangy, and Anastassia V. Komarova

Correspondence

frederic.tangy@pasteur.fr;
stasy@pasteur.fr

In Brief

Control of measles virus infection and measles-based oncolytic therapy are possible, thanks to the existence of a safe and efficient live attenuated vaccine. Molecular mechanisms that make this vaccine to be so efficient are yet to be determined. We show that the measles C protein is responsible for the establishment of complex networks of interactions with the host cell. We suggest that the C protein binding to the p65–iASPP protein complex controls the host cell death and innate immunity pathways.

Graphical Abstract
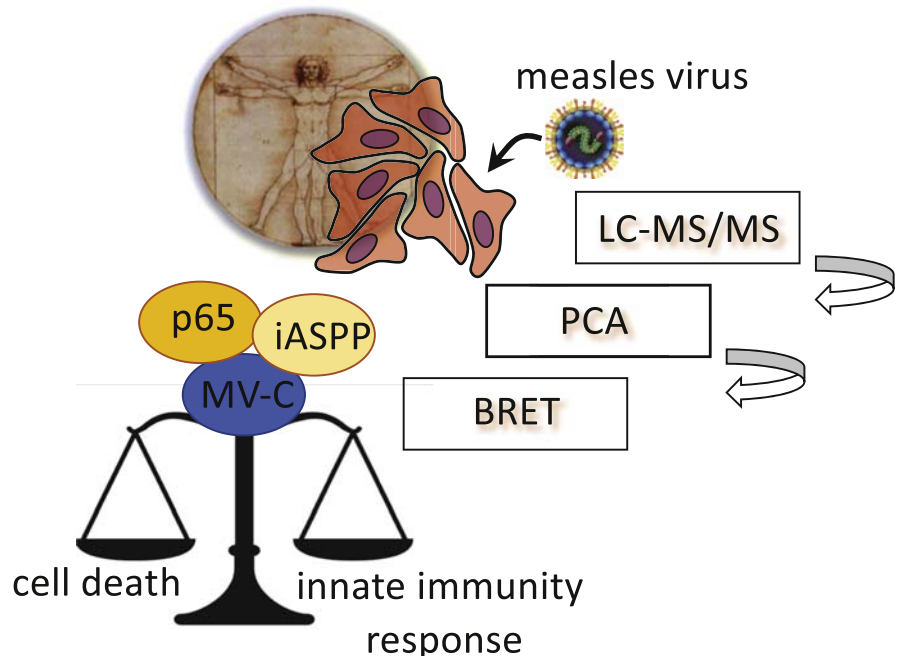
Highlights

- Measles virus controls immune response and cell death pathways to achieve replication.

- Host proteins interaction network with measles virulence factor C protein.

- Cellular p65–iASPP complex is targeted by measles virus C protein.

Proteomic Analysis Uncovers Measles Virus Protein C Interaction With p65–iASPP Protein Complex

Alice Meignié[1,2,‡], Chantal Combredet[1,‡], Marc Santolini[3,4], István A. Kovács[4,5,6], Thibaut Douché[7], Quentin Giai Gianetto[7,8], Hyeju Eun[9], Mariette Matondo[7], Yves Jacob[10], Regis Grailhe[9], Frédéric Tangy[1,*], and Anastassia V. Komarova[1,10,*]

Viruses manipulate the central machineries of host cells to their advantage. They prevent host cell antiviral responses to create a favorable environment for their survival and propagation. Measles virus (MV) encodes two nonstructural proteins MV-V and MV-C known to counteract the host interferon response and to regulate cell death pathways. Several molecular mechanisms underlying MV-V regulation of innate immunity and cell death pathways have been proposed, whereas MV-C host-interacting proteins are less studied. We suggest that some cellular factors that are controlled by MV-C protein during viral replication could be components of innate immunity and the cell death pathways. To determine which host factors are targeted by MV-C, we captured both direct and indirect host-interacting proteins of MV-C protein. For this, we used a strategy based on recombinant viruses expressing tagged viral proteins followed by affinity purification and a bottom-up mass spectrometry analysis. From the list of host proteins specifically interacting with MV-C protein in different cell lines, we selected the host targets that belong to immunity and cell death pathways for further validation. Direct protein interaction partners of MV-C were determined by applying protein complementation assay and the bioluminescence resonance energy transfer approach. As a result, we found that MV-C protein specifically interacts with p65–iASPP protein complex that controls both cell death and innate immunity pathways and evaluated the significance of these host factors on virus replication.

Measles virus (MV) is a member of the genus *Morbillivirus* of the family *Paramyxoviridae*. This enveloped virus with a negative-sense nonsegmented RNA genome is responsible for measles, a childhood disease that used to cause 2.6 million deaths each year globally before the introduction of a live attenuated vaccine in the 1970s that reduced the incidence of the disease by 95%. Since then, the MV vaccine has shown its safety and efficacy in over two billion children ([1]). However, despite almost 50 years of vaccination history, we still know little about molecular mechanisms that make the attenuated MV vaccine so efficient. Furthermore, the measles vector platform is a promising plug-and-play vaccine platform technology for the rapid development of effective preventive vaccines against viral and other infectious diseases ([1]). Another strong argument to study molecular mechanisms of MV replication and cellular pathways that are launched or controlled by MV is the efficacy of the MV vaccine for oncolytic viral therapy ([2]). Thus, numerous fundamental studies are needed to understand the principles of MV vaccine functioning as a preventive and therapeutic agent.

MV genome contains six genes encoding six structural proteins (N-P-M-F-H-L). The P gene encodes the P protein and two accessory proteins: V ([3]) and C ([4]). Both MV-V and MV-C are viral virulence factors that exert multiple regulatory functions, suggesting numerous dynamic interactions with the human proteome. MV-V counteracts the host type I interferon (IFN) response by interacting with melanoma differentiation–associated protein 5, laboratory of genetics and physiology 2, nuclear factor-kappa B (NF-κB) subunits p65, IκB kinase α, signal transducer and activator of transcription 1 and 2, and Janus kinase 1 and by interfering with their functions ([5–8]).

MV-V also interacts with p53 and p73 proteins, suggesting a link between MV-V and the cellular apoptosis pathway (9, 10). By interacting with TRIpartite motif–containing protein 25, MV-V stops the antiviral activities of retinoic acid–inducible gene I (RIG-I) in the type I IFN signaling pathway (11). Numerous host-interacting proteins have therefore been validated for MV-V, whereas the MV-C network of interactions within infected cells remains undetermined.

Viruses in the genera *Respirovirus, Henipavirus, and Morbillivirus* and *Tupaia paramyxovirus*–like viruses within the *Paramyxoviridae* family express one or more C proteins, which are relatively small basic proteins translated from the P mRNA in a different open frame from that for the P protein (12). MV-C is a highly positively charged protein of 186 AA (4). Using immunofluorescence, MV-C was localized in the nucleus and cytoplasmic inclusions (4, 13, 14). MV-C possesses a nuclear localization signal and a nuclear export signal, which allow MV-C to shuttle between the cytoplasm and the nucleus (14).

MV with an abrogated expression of the C protein (MVΔC) has been evaluated *in vitro* and *in vivo* (15–24). In nonhuman primates, MV-C can prevent cell death and is necessary for efficient viral replication as dramatically reduced expression of an MV antigen is detected in different tissues in comparison with WT MV (15, 24). MV-C protein has been reported to inhibit the IFN-α/β/γ responses (25–27). MV-C interferes with the induction of IFN at the transcriptional level (28) and seems to control the induction of IFN by regulating viral RNA synthesis (21, 22, 29–31).

Numerous studies have demonstrated that viral defective interfering (DI) genomes are accumulated upon cell infection with MVΔC virus (21, 32). These truncated replicative forms of the viral genome are directly linked to type I IFN signaling through RIG-I and protein kinase R (PKR) (22, 32–35). Indeed, RIG-I is one of the viral RNA sensors triggering the production of proinflammatory cytokines, including IFN-α/β, and the establishment of an antiviral state in the host cells (36). PKR is another sensor of viral dsRNA. Its activation triggers a cellular stress response leading to downregulation of cellular protein synthesis because of the phosphorylation of eukaryotic translation initiation factor 2α and to the formation of stress granules (36). In addition, the enhanced production of MV DI genomes by MVΔC that mediates PKR has correlated with a better activation of IFN regulatory factor 3, NF-κb, and activating transcription factor 2 that increase IFN production (33). Thus, MV-C deletion from the virus suggests a direct contribution of MV-C on the viral RNA synthesis and either indirect or direct control of the host's innate immune responses.

In cell culture, MV infection induces autophagy that is likely to favor the production of MV infectious particles and to delay the apoptosis induced by viral replication (23, 37). MVΔC does not induce autophagy. Thus, it presents a defect in replication and is more apoptotic than the WT virus (23, 38). Former studies have also indicated that another paramyxovirus, the Sendai virus, induces apoptosis, lacking expression of the C protein or containing a mutated C protein (39, 40). These results suggest that MV replication induces apoptosis and that MV-C protein blocks this process *via* the modulation of virus replication process or *via* interaction with yet to be determined host factors.

To determine the MV-C interaction network with host proteins, we captured both direct and indirect interacting proteins of MV-C protein expressed during the infection. For this, we used a strategy based on recombinant viruses expressing tagged viral protein followed by affinity purification and a bottom-up mass spectrometry–based proteomics analysis (10). A list of specific MV-C protein–protein interactions (PPIs) was established in different cell lines, from which we validated MV-C direct PPI with proteins that belong to the immunity and cell death pathways. In particular, we uncovered MV-C direct PPIs with the p65–iASPP protein complex that provide a mechanism on how MV-C protein can control both immunity and cell death responses.

EXPERIMENTAL PROCEDURES

Cells

HEK293T (human embryonic kidney), HeLa (adenocarcinomic human epithelial cells), A549 (adenocarcinomic human alveolar basal epithelial cells), and Vero cells (African green monkey kidney cells) were maintained in Dulbecco's modified Eagle's medium (DMEM), high glucose, GlutaMAX (#61965, Fisher Scientific) supplemented with 10% fetal bovine serum (#35-0789-CV, Corning), and 100 units/ml of penicillin and 100 μg/ml of streptomycin (#P4333, Sigma-Aldrich) at 37 °C in a 5% CO_2 humidified atmosphere.

The 293T KO cell lines were generated by cotransfection (lipofectamine 2000, Invitrogen) of CRISPR–Cas9–expressing KO plasmids (p65: sc-400004-ko-2, iASPP: sc-404703, p53: sc-416469, and control: sc-418922 from Santa Cruz). The KO plasmids are a mixture of three plasmids, each carrying a different guide RNA specific for the target gene, as well as the Cas- and GFP-coding regions. Forty-eight hours after transfection, GFP-positive cells were selected by cell sorting. The depletion of target proteins was verified by Western blotting.

Plasmid Constructions

For recombinant virus cloning, construction of plasmids pTM-MVSchw, which contain an infectious MV cDNA corresponding to the antigenome of the Schwarz MV vaccine strain, has been described elsewhere (41).

To generate plasmids expressing a STrEP-tagged (WSHPQFEK) MV-C with an additional transcription unit (ATU) in between the H and L genes (ATU3, Fig. 1A), a two-step PCR-based strategy was used to produce coding sequences for MV-C and the Red Fluorescent Protein Cherry (Ch) with either N- or C- terminal One-STrEP-tags. First, the One-STrEP-tag coding sequence was amplified by PCR from pEXPR-IBA105 using different primer pairs to add a flexible Tobacco Etch Virus protease linker (ENLYFQS) either at the N- or C- terminal to this sequence. In parallel, DNA fragments corresponding to MV-C or Ch coding sequences were amplified using pTM3-MVSchw or pmCherry (Clontech) as a template. PCR products were finally combined and then amplified in a second PCR to recover expected fused sequences, that is, MV-C with either N-terminal or C-terminal One-STrEP-tag and CH with only N-terminal One-STrEP-tag. These three amplicons that

contained unique *Bsi*WI and *Bss*HII sites at their extremities were first cloned in pCR2.1-TOPO plasmid (Invitrogen) and Sanger sequenced. These plasmids were designated pTOPO/STrEP-C, pTOPO/C-STrEP, and pTOPO/STrEP-Ch. Finally, sequences were introduced in the ATU3 of pTM3-MVSchw vector (41) after *Bsi*WI/*Bss*HII digestion. The resulting plasmids were designated pTM3-MV/STrEP-C, pTM3-MV/C-STrEP, and pTM3-MV/STrEP-Ch. All MV insertions respect the "rule of six," which stipulates that the number of nucleotides of MV genome must be a multiple of six (42). Recombinant viruses were rescued, and virus titers and single-step growth curves were determined as described previously (41).

For protein complementation assay (PCA) based on the split luciferase (N2H) vectors pSNL-N1 and pSNL-N2 expressing the nano-luciferase (Nluc)1 and Nluc2, complementary fragments of Nluc linked to the N-terminus of tested proteins were used (43). The ORFs encoding for the selected proteins (Supplemental Table S1) cloned into vector pDON223 (Gateway system, Invitrogen) by recombination cloning (Gateway system, Invitrogen) were collected from human ORFeome Collection v8.1 (a generous gift from Center for Cancer Systems Biology, Dana-Farber Cancer Institute, Harvard Medical School, Boston). The resulting entry clones were then transferred into Gateway-compatible PCA destination vector pSNL-N1. The resulting pSNL-N1-"C interactors" were sequenced using a forward primer (5′-GCTGAAGATCGACATCCATGTC-3′). The sequences were compared with the human genome by performing a BLAST search to identify the cDNA and the isoform when it is known. The in-frame fusion with the Nluc1 fragment of Nluc was verified. The ORFs encoding the MV-C protein and Muc7 protein (mucin 7 was used as a negative control) were cloned into the entry vector pDON207 (Gateway system, Invitrogen). They were transferred into the destination vector pSNL-N2 by Gateway cloning. The resulting pSNL-N2-C and pSNL-N2-Muc7 were sequenced using a forward primer (5′-CGGAGTGACCGGCTGGCGGCTG-3′).

For bioluminescence resonance energy transfer (BRET) assay, we used the pEYFP-C1/N1 plasmids encompassing EYFP tag in the N- or C-terminal positions (Clontech). To obtain pNluc-C1/N1 plasmids, the pEYFP-C1/N1 plasmids were modified by replacing the EYFP with the Nluc coding sequence. A simple PCR amplification strategy was used to clone MV-C and p53 coding sequences in either pNluc-C1/N1 or pEYFP-N1 expression vectors. p53 was amplified from the spleen cDNA library (Invitrogen). MV-C was amplified from pTM-Schwarz using different primers: forward 5′-TTCGAATTCTATGTCAAAAACGGA and reverse 5′-TAAGCGCGCGTCGACTCAGGAGCTCGTGGAT, digested with *Eco*RI and *Sal*I DNA restriction endonucleases and cloned in pNluc-C1 vector. A similar protocol was used to obtain pNluc-N1-MVC plasmid, except that primers were forward 5′-TTA-GAATTCGCCACCATGTCAAAAACGGAC and reverse 5′-TAAGTC-GACTGGGAGCTCGTCGTGGA and the vector was pNluc-N1. The same protocol was repeated to obtain pEYFP-N1-p53 plasmid encoding p53 with forward 5′-TTAGAATTCATGGAGCCGCAGTCAGA and reverse 5′-AATGTCGACGTCTGAGTCAGGCCCTTCTG primers. The resulting plasmids were designated as Nluc-C, C-Nluc, and YFP-p53. iASPP-YFP was obtained by recombination cloning (Gateway system), and pDON223-iASPP was then transferred into a Gateway-compatible destination vector pEYFP-C1. Plasmids were Sanger sequenced using the CMV promoter primer. pYFP-p65 which contains EYFP reporter gene fused to p65 was a kind gift of Dr Hervé Bourhy from Lyssavirus Epidemiology and Neuropathology Laboratory of Institut Pasteur (44). BRET negative-control plasmids cSOD1-YFP, SOD1-Nluc, and YFP-Nluc have been described elsewhere (45).

Viruses

The MV Schwarz vaccine strain (MVSchw, GenBank accession no. AF266291.1) was described in Combredet *et al.* (41). rTM3-MV/STrEP-C, rTM3-MV/C-STrEP, and TM3-MV/STrEP-Ch plasmids were used to rescue corresponding viruses using the helper cell–based rescue system described in Combredet *et al.* (41). rMVΔC has been described previously in Mura *et al.* (32). Virus stocks were produced by virus multiplication on Vero cells at a multiplicity of infection (MOI) of 0.1. Virus titers were determined by TCID50 titration on Vero cells as described previously in Guerbois *et al.* (46).

Antibodies

As primary antibodies, we used rabbit polyclonal anti-MV-C (kindly provided by Dr Kaoru Takeuchi [47]), a rabbit polyclonal NF-κB p65 antibody (ab16502, Abcam), a mouse monoclonal p53 antibody (PAb 240, Invitrogen), a mouse monoclonal antibody iASPP (sc-398566, Santa Cruz), a mouse anti-p53 (556534, BD Biosciences), a mouse anti-N mAb (clone 25; kindly provided by Pr Chantal Rabourdin-Combe, [48]), monoclonal mouse Strep-tag antibodies (#34850, Qiagen), and a monoclonal anti-actin antibody (A5441, Sigma-Aldrich). As secondary antibodies, we used for Western blot a goat anti-mouse immunoglobulins HRP-conjugated (P0447, Dako) or anti-rabbit (P0399, Dako), for immunofluorescence, a goat anti-mouse IgG (H + L) secondary antibody Alexa Fluor 555 (#A31572, Thermo Fisher Scientific) and a goat anti-rabbit IgG (H + L) highly cross-adsorbed secondary antibody Alexa Fluor 647 (#A21240, Thermo Fisher Scientific), and for flow cytometry analysis, an anti-Measles antibody, nucleoprotein, clone 83KKII, FITC-conjugated (#MAB8906F, Sigma-Aldrich).

Western Blot Assays

A549, HeLa, or HEK293T cells were mock-infected (treated with media alone) or infected for 24 h with MV recombinant viruses at an MOI of 1. Protein lysates were fractionated by SDS-PAGE on 4 to 12% NuPAGE Bis-Tris gels (#WG1401BOX, Thermo Fisher Scientific) with Mops running buffer (#NP0001, Thermo Fisher Scientific) and transferred to cellulose membranes (#10600018, GE Healthcare). Peroxidase activity was visualized with SuperSignal West Pico PLUS Chemiluminescent Substrate (#34580, Thermo Fisher Scientific).

Flow Cytometry

HEK293T, HeLa, and A549 (2×10^5 cells per well) were plated in a 24-well plate and infected at an MOI 1 with the corresponding recombinant viruses. Cells were washed twice with Dulbecco's PBS (#14190, Thermo Fisher Scientific) and 2% fetal calf serum and then fixed in PBS containing 4% paraformaldehyde. Cells were permeabilized with Perm/Wash buffer (#554723, BD Biosciences), incubated with the primary antibody anti-N at 4 °C for 30 min, washed in Perm/Wash, and incubated with the secondary antibody anti-mouse. Cells were washed twice with PBS 2% fetal calf serum before analysis by flow cytometry using a MACSQuant cytometer (Miltenyi Biotec), and the analysis was performed with the software FlowJo (version 7.6).

Affinity Purification of MV-C–Specific Protein Complexes

HEK293T, HeLa, and A549 (2×10^7 cells per well) were mock-infected (treated with media alone) or infected at an MOI of 1 for 24 h with MV-Schwarz, rTM3-MV/C-STrEP, rTM3-MV/STrEP-C, and rTM3-MV/STrEP-Ch. Cells were washed twice with cold PBS and lysed in 4 ml of the lysis buffer (20-mM Mops-KOH, pH 7.4, 120-mM of KCl, 0.5% IGEPAL, 2-mM β-mercaptoethanol), supplemented with complete EDTA-free protease inhibitor cocktail (#11836170001 or #11873580001, Roche Diagnostics). Cell lysates were incubated on ice for 20 min with gentle mixing every 5 min, and then clarified by centrifugation at 16,000*g* for 15 min at 4 °C. The clarified cell lysates were incubated for 2 h on a spinning wheel at 4 °C with 100 μl of

StrepTactin Sepharose High Performance beads (#28935599, GE Healthcare). Beads were collected by centrifugation (1600g for 5 min at 4 °C) and washed twice for 5 min on a spinning wheel with 5 ml of the washing buffer (20-mM Mops-KOH, pH 7.4, 120 mM of KCl, 2-mM β-mercaptoethanol) supplemented with complete protease inhibitor cocktail. Proteins were eluted using 200-μl StrepTactin elution buffer with Biotin (#2-1019-025, IBA). Finally, eluted proteins were precipitated overnight at 4 °C with trichloroacetic acid (12% final concentration). Protein pellets were washed twice with ice-cold acetone and resuspended in urea 8 M, 4% SDS final solution, or were analyzed either by Western blotting or by LC-MS/MS. For each cell line, three independent biological replicates of cell infection followed by affinity purification of MV-C–specific protein complexes were performed.

LC-MS/MS Analysis

For MV-C–specific protein cocomplex (OUTPUTS), the digestion of the protein pellets was resuspended in 45 μl of a urea 8 M/NH_4HCO_3 100-mM denaturation buffer and sonicated 2 × 1 min on ice. Cysteine bonds were reduced with 50-mM tris (2-carboxyethyl) phosphine (#646547, Sigma-Aldrich) for 1 h and alkylated with 50-mM iodoacetamide (#I114, Sigma-Aldrich) for 1 h at room temperature in the dark. Samples were digested with rLys-C (#V1671, Promega) ratio 50:1 (protein:rLysC) for 3 h/37 °C and then digested with Sequencing Grade Modified Trypsin (#V5111, Promega) ratio 50:1 (protein:trypsin) overnight at 37 °C. The digestion was stopped with 4% formic acid (FA) (#94318, Fluka) and digested peptides were purified with C18 Spin Columns Pierce (#89870, Thermo Fisher Scientific). Peptides were eluted with 2× 80% acetonitrile (ACN)/0.1% FA. The resulting peptides were SpeedVac-dried and resuspended in 2% ACN/0.1% FA.

For input sample digestion, clarified cell lysates were processed as described (49). Briefly, 30,000 molecular weight cut-off centrifugal units (Amicon Centrifugal Filters, Merck) and collection tubes were passivated in 5% (v/v) TWEEN 20, and all subsequent centrifugation steps were carried out at 14,000g for 10 min. For each sample, 50 μg of proteins were transferred into a filter unit and the lysis buffer was exchanged with an exchanged buffer composed of 8 M urea, 0.2% dichloroacetic acid (DCA), 100-mM ammonium bicarbonate, pH 8.0. Disulfide bonds were reduced with 5-mM tris (2-carboxyethyl) phosphine for 1 h and then alkylated with 50-mM iodoacetamide in the dark for 1 h. Finally, one exchange buffer and two washes with the digestion buffer (0.2% DCA/50-mM ammonium bicarbonate, pH 8) were performed before adding 100 μl of the digestion buffer containing 1:50 ratio of sequencing-grade modified trypsin. Proteolysis was carried out at 37 °C overnight and peptide recovery was performed with 50-mM ammonium bicarbonate, pH 8.0. DCA was removed by acidification and phase transfer. Finally, dried peptides were resuspended in 2% ACN and 0.1% FA before LC-MS/MS analysis.

LC-MS/MS analysis of MV-C–specific protein complexes was performed on a Q Exactive Plus Mass Spectrometer (Thermo Fisher Scientific) coupled with a Proxeon EASY-nLC 1000 (Thermo Fisher Scientific). Three hundred fifty nanograms of peptides were injected onto a homemade 50-cm C18 column (1.9-μm particles, 100-Å pore size, ReproSil-Pur Basic C18, Dr Maisch GmbH, Ammerbuch-Entringen) and eluted with a multistep gradient from 2 to 27% ACN in 105 min, 27 to 50% ACN in 40 min, and 50 to 60% ACN in 10 min, at a flow rate of 250 nl/min over 185 min. The column temperature was set to 60 °C. MS data were acquired using Xcalibur software using a data-dependent method. MS scans were acquired at a resolution of 70,000 and MS/MS scans (fixed first mass 100 m/z) at a resolution of 17,500. The automatic gain control (AGC) target and maximum injection time for the survey scans and the MS/MS scans were set to 3E6, 20 ms and 1E6, 60 ms, respectively. An automatic selection of the ten most intense precursor ions was activated (top 10) with a 45-s

dynamic exclusion. The isolation window was set to 1.6 m/z and normalized collision energy fixed to 28 for higher energy collisional dissociation fragmentation. We used an underfill ratio of 1.0% for an intensity threshold of 1.7E5. Unassigned precursor ion charge states as well as 1, 7, 8, and >8 charged states were rejected, and peptide match was disabled.

LC-MS/MS analysis of clarified total lysates (INPUTS) was performed on a Q Exactive Plus Mass Spectrometer (Thermo Fisher Scientific) coupled with a Proxeon EASY-nLC 1200 (Thermo Fisher Scientific). 1 μg of peptides were injected onto a homemade 50-cm C18 column (1.9-μm particles, 100-Å pore size, ReproSil-Pur Basic C18, Dr Maisch GmbH, Ammerbuch-Entringen, Germany) and eluted with a multistep gradient from 3 to 29% buffer B (80% ACN) in 135 min, 29 to 56% buffer B in 20 min, and at a flow rate of 250 nl/min over 182 min. The column temperature was set to 60 °C. MS data were acquired using Xcalibur software using a data-dependent method. MS scans were acquired at a resolution of 70,000 and MS/MS scans (fixed first mass 100 m/z) at a resolution of 17,500. The AGC target and maximum injection time for the survey scans and the MS/MS scans were set to 3E6, 20 ms and 1E6, 60 ms, respectively. An automatic selection of the ten most intense precursor ions was activated (top ten) with a 45-s dynamic exclusion. The isolation window was set to 1.6 m/z and normalized collision energy fixed to 28 for higher energy collisional dissociation fragmentation. We used a minimum AGC target of 1.0E4 corresponding to an intensity threshold of 1.7E5. Unassigned precursor ion charge states as well as 1, 7, 8, and >8 charged states were rejected, and peptide match was disabled.

Bioinformatics Analysis of LC-MS/MS Data

Raw data were analyzed using MaxQuant software version 1.5.0.30 (50) for output samples and version 1.5.1.2 for inputs using the Andromeda search engine (51). The MS/MS spectra were searched against two databases: the Human Swiss-Prot database (20,203 entries from the UniProt, 18/08/2015) and the *Morbillivirus* Swiss-Prot database (90 entries from the UniProt, 12/01/2016). Variable modifications (methionine oxidation and N-terminal acetylation) and fixed modification (cysteine carbamidomethylation) were set for the search, and trypsin with a maximum of two missed cleavages was chosen for searching. The minimum peptide length was set to seven amino acids, and the false discovery rate (FDR) for peptide and protein identification was set to 0.01. At least a unique peptide per protein group was required for the identification of the proteins. The main search peptide tolerance was set to 4.5 ppm and 20 ppm for the MS/MS match tolerance. Second peptides were enabled to identify cofragmentation events and match between runs option selected with a match time window of 0.7 min for an alignment time window of 20 min. Quantification was performed using the XIC-based LFQ algorithm with the Fast LFQ mode as described previously (52). Unique and razor peptides, including modified peptides, with at least 2 ratio counts, were accepted for quantification. Three MaxQuant analyses were computed and analyzed separately to the three different cell lines studied (HeLa, A549, and HEK 293T cell lines), respectively.

The mass spectrometry proteomics data have been deposited to the ProteomeXchange Consortium *via* the PRIDE (53) partner repository with the data set identifier PXD015316.

Statistical Analysis

For the differential analyses, proteins identified in the reverse and contaminant databases and proteins "only identified by the site" were first discarded from the list of identified proteins. Then, only proteins with three quantified intensity values in a condition were kept. After log2 transformation of the leftover proteins, LFQ values were normalized by median centering within conditions (normalizeD function of the R package DAPAR [54]). Remaining proteins without any

LFQ value in one of both conditions have been considered as proteins quantitatively present in a condition and absent in another. They have therefore been set aside and considered as differentially abundant proteins. Next, missing values were imputed using the imp.norm function of the R package norm (Novo A. A. norm: Analysis of multivariate normal data sets with missing values. 2013 R package version 1.0–9.5). Proteins with a fold change under 2.0 have been considered not significantly differentially abundant. Statistical testing of the remaining proteins (having a fold change over 2.0) was conducted using a limma *t* test (55) using the R package limma (56). An adaptive Benjamini-Hochberg procedure was applied on the resulting *p*-values, thanks to the function adjust.*p* of R package cp4p (57) using the robust method of (56) to estimate the proportion of true null hypotheses among the set of statistical tests. The proteins associated with an adjusted *p*-value inferior to an FDR of 1% have been considered as significantly differentially abundant proteins. Finally, the proteins of interest are therefore those which emerge from this statistical analysis supplemented by those which are considered to be present from one condition and absent in another. For statistical analysis of output samples for a protein to be considered as a positive hit, it needed to be detected in each of the three biological replicates. For total lysate (INPUTS) data analysis, positive hits are proteins that were detected in at least two biological replicates.

Constructing the Human Protein–Protein Interactome

We assembled 15 commonly used databases, focusing on high-quality PPIs with five types of evidence: (1) binary, physical PPIs tested by high-throughput yeast two-hybrid (Y2H) screening system, combining binary PPIs tested from three publicly available high-quality Y2H data sets (58–60), (2) literature-curated PPIs identified by affinity purification followed by affinity purification mass spectrometry, Y2H, and literature-derived low-throughput experiments; (3) binary, physical PPIs derived from protein three-dimensional structures; (4) kinase–substrate interactions by literature-derived low-throughput and high-throughput experiments; and (5) signaling networks by literature-derived low-throughput experiments. The protein-coding genes were mapped to their official gene symbols based on Gene-Cards (http://www.genecards.org/) and their Entrez ID. Computationally inferred interactions rooted in evolutionary analysis, gene expression data, and metabolic associations were excluded. The updated human interactome includes 243,603 PPIs connecting 16,677 unique proteins and is 40% greater in size than the previously used human interactome (61). The human protein–protein interactome is provided in Supplemental Data (62).

PCA Based on the Split Luciferase

HEK293T cells were seeded in a white-bottom 96-well flat microplate (#655083, CELLSTAR, Greiner Bio-One) at a concentration of 4.0×10^4 cells per well. After 24 h, cells were transfected using PEI MAX (#24765-1, Polysciences) with 100 ng of pSNL-N2-C or pSNL-N2-Muc7 and 100 ng of pSNL-N1-"C interactors." At 24 h, post-transfection media was removed and Nluc enzymatic activity was measured using a Berthold Centro-XS luminometer by injecting 50 μl of luciferase substrate reagent (#E2820, Promega) per well and counting luminescence for 2 s. Results were expressed as relative light units or as a fold change normalized over the sum of controls, specified herein as normalized luminescence ratio (NLR). For a given protein pair A/B, NLR = (Nluc1-A + Nluc2-B)/[(Nluc1-A + Nluc2) + (Nluc1 + Nluc2-B)]. For the NLR validation experiment, each protein pair was assessed three times or more. The NLR of the protein pair was considered as 'validated' if above a threshold value of log(NLR) of 1.55 and above the upper limit of the confidence interval defined for the Muc7/bait pairs.

BRET

HEK293T cells were seeded in 384-well (4000 cells/well) flat-bottom μClear plates (#781097, Greiner Bio-One) coated with fibronectin (#354008, BD Biosciences). Transfection of HEK293T cells was performed at 80% confluence using 25 ng of each plasmid construction mixed with 150 nl of FuGENE 6 (E2691, Promega) reagent per well. Twenty four hours after transfection, fluorescence imaging measurements were performed using an Operetta widefield HCS system (Perkin Elmer) equipped with a Peltier-cooled CCD camera with 1.3 megapixels per frame, 14-bit resolution, and a 20× long working distance objective lens with a 0.45 numerical aperture. Then, the media was removed and replaced by DMEM without phenol red (#21063029, Gibco, Switzerland), supplemented with the assay substrate Nano-Glo containing the furimazine at 200-fold dilution (#N1110, Promega). The bioluminescence signal of Nluc donor and the YFP acceptor emission were acquired using an EnVision Multimode Plate Reader (Perkin Elmer) sequentially using a low and high band-pass filter (460/25 nm, 535/25 nm), with an acquisition time of 0.5 s. In addition, emission spectral scans of the HEK293T cells expressing recombinant Nluc fusions positive and negative control were performed using a SpectraMax M5 fluorescence microplate reader (Molecular Devices). Emission spectra were recorded from 350 nm to 700 nm using an integration time of 500 ms with 1-nm step increments. All spectra were normalized to the luminescence value at the emission maximum (449 nm) of Nluc. netBret was calculated using the method outlined in Kim *et al.* (45).

$$Cf = \frac{BL(Acceptor\ filter)donor\ only}{BL(Donor\ filter)donor\ only}$$

$$net\ BRET = \frac{[BL(Acceptor\ filter) - Cf \times BL(Donor\ filter)]}{BL(Donor\ filter)}$$

where BL is bioluminescent.

Experimental Design and Statistical Rationale

For each experimental condition, three biological replicates were performed and analyzed each time. For mass spectrometry, MV-Ch–infected cells were analyzed as a control to remove all nonspecific interactions.

RESULTS

Generation and Characterization of Recombinant MV Expressing a Tagged MV-C

To copurify MV-C with associated protein complexes from infected cells, we expressed MV-C from MV genome with a fusion tag allowing its capture. To reach this goal, we took advantage of reverse genetics for cloning and rescuing genetically modified MV (41) and of our specific proteomic approach to study host-interacting partners of viral proteins in infected cells (10). Both N- and C-terminal tags were considered. Sequences encoding the MV-C protein with N- or C-terminal One-STrEP-tag were inserted into the pTM-MVSchw plasmid that contains a full-length infectious MV genome (41). Expressing additional copies of MV-C from infectious MV appeared difficult. Indeed, expression from an ATU located downstream of the P gene (ATU2) (Fig. 1A) was impossible after numerous attempts for either N- or C-terminally tagged C protein. Most rescued viruses either had stop codons that
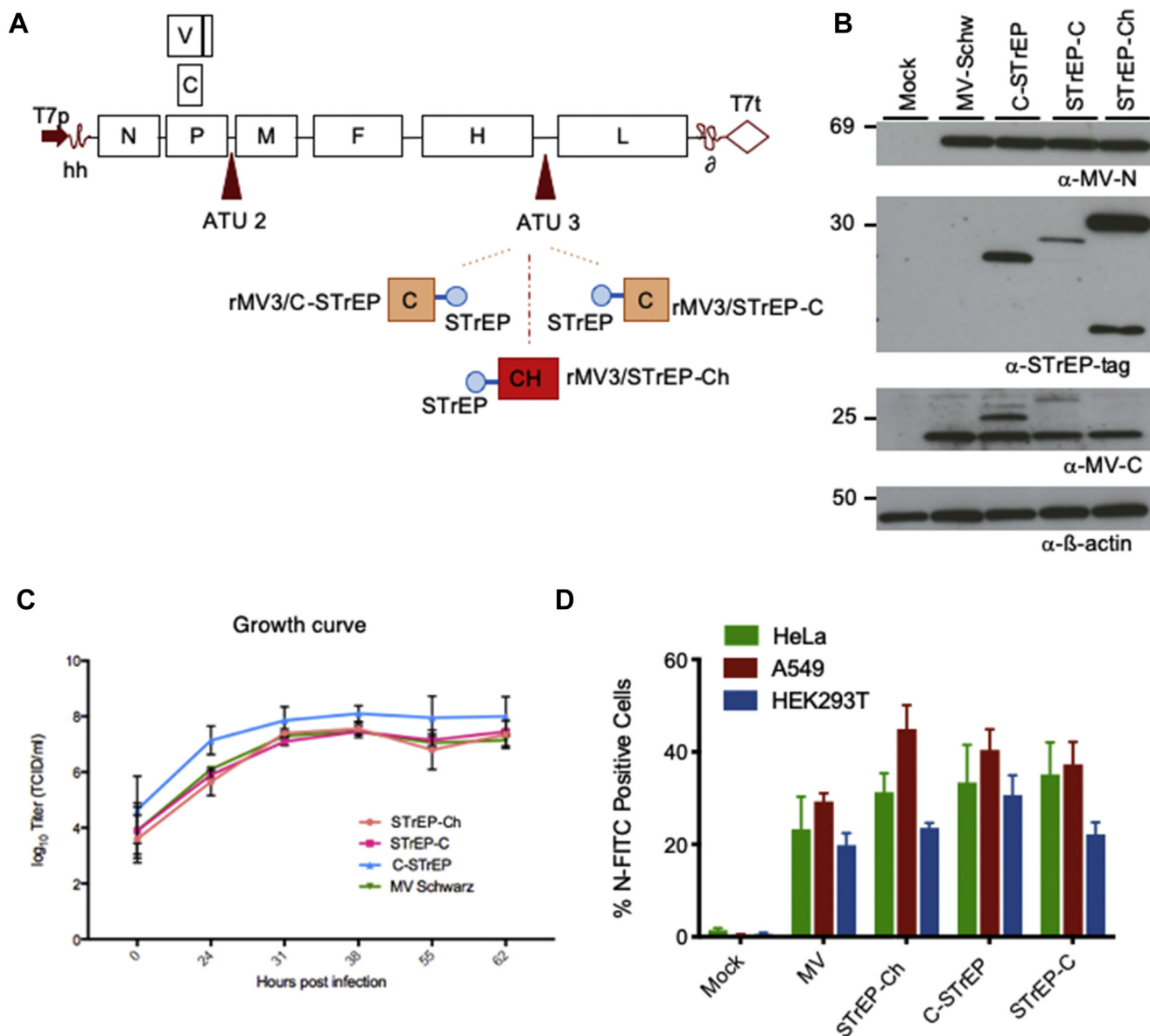
FIG. 1. **Recombinant viruses express tagged MV-C proteins and replicate at high titers.** *A*, schematic representation of recombinant virus genomes. MV negative-sense RNA genome is displayed with its 3′ end on the *left*, with the six genes indicated by *capital letters* and depicted as *rectangles*. The additional transcriptional units encoding for One-STrEP-tagged MV-C (STrEP-C or C-STrEP) or mCherry protein (STrEP-Ch) are inserted between H and L genes. The *blue oval* represents the One-STrEP-tag sequence. T7p is a T7 RNA polymerase promoter sequence, hh is a hammerhead ribozyme, T7t is a T7 RNA polymerase termination signal, δ is a hepatitis delta ribozyme. *B*, HeLa cells were infected with the native MVSchw strain, or the rMV2/STrEP-C and rMV2/C-STrEP expressing the One-STrEP-tagged MV-C protein or the rMV2/STrEP-Ch expressing the One-STrEP-tagged Ch protein. Expressions of native and One-STrEP-tagged MV-C proteins were determined by Western blot using anti-C polyclonal and anti-STrEP tag monoclonal antibodies, respectively. Anti-MV-N antibody and anti-β-actin served as controls for measles infection and loading, respectively. *C*, virus growth curves obtained for rMV2/STrEP-C and rMV2/C-STrEP and rMV2/STrEP-Ch. MV Schwarz strain was used as a control. Vero cells were infected with MV Schwarz, rMV2/STrEP-C, and rMV2/C-STrEP, or rMV2/STrEP-Ch at an MOI of 0.1. Cell-associated virions were recovered at each time point, and titers were determined using the TCID50 method. Two biological experiments were performed, and each point represents the mean and SD of the two values. *D*, the efficiency of tagged recombinant virus replication in HEK293T, HeLa, and A549 cells analyzed by fluorescence-activated cell sorting. Cells were infected at MOI of 1. 24 h after infection, cells were harvested, fixed, and stained using an anti-N antibody to measure the percentage of N positive cells. Experiments were performed two times, and data represent the means ± SD of the technical triplicates of the most representative experiment. MOI, multiplicity of infection; MV, measles virus.
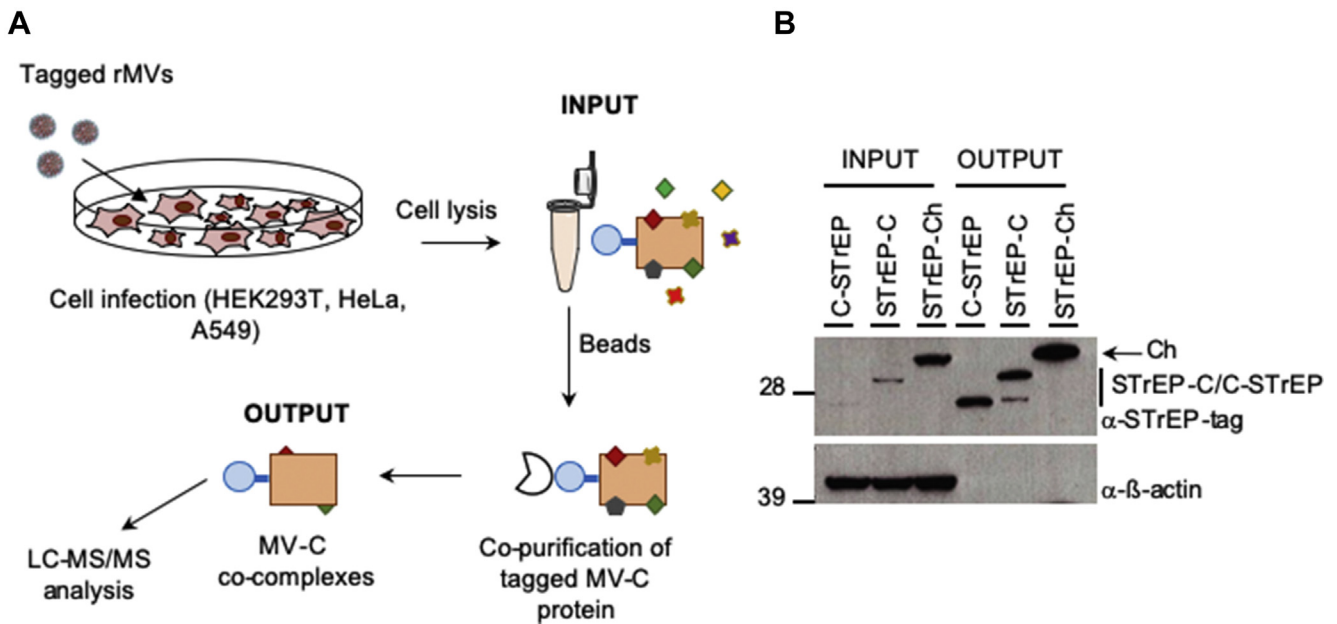
A

B

FIG. 2. **rMV3/STrEP-C and rMV3/C-STrEP recombinant viruses allow purification of MV-C–specific protein co-complexes.** *A*, the protocol used to purify STrEP-C and associated cellular proteins from the infected cell for MS analysis of MV-C–specific protein factors. HEK293T, HeLa, and A549 cells were infected with the corresponding recombinant tagged viruses. At 24 h after infection, cells were lysed, and STrEP-C, C-STrEP, and STrEP-Ch were copurified with interacting cellular proteins using StrepTactin Sepharose beads. After two subsequent washing steps, protein complexes were released from the beads and prepared for LC-MS/MS. *B*, HEK293 T cells were infected with rMV3/STrEP-Ch, rMV3/STrEP-C, or rMV3/C-STrEP. Total lysates (INPUT) and MV-C–specific protein complexes (OUTPUT) were analyzed by Western blot using the One-STrEP-tag antibody. Western blot analysis of β-actin served as a control for loading and nonspecific binding. MV, measles virus.

blocked the expression of the second copy of MV-C or introduced numerous mutations within MV-C coding sequence (data not shown). However, we succeeded in introducing an additional copy of MV-C gene with N- or C-terminal One-STrEP-tag in ATU3 located downstream of the H gene (Fig. 1*A*). Recombinant viruses encoding One-STrEP-tagged MV-C protein were rescued, and polyclonal population of each recombinant virus was obtained. Modified recombinant viruses were designated rMV3/C-STrEP and rMV3/STrEP-C, respectively. As a negative control, we generated N-terminally tagged recombinant virus expressing the red fluorescent protein (Cherry, Ch) from ATU3 (designated rMV3/STrEP-Ch).

To validate the expression of MV-C and Ch-tagged proteins from rMV3/C-STrEP, rMV3/STrEP-C, and rMV3/STrEP-Ch, HeLa cells were infected with recombinant viruses at an MOI of 1, and protein expression was determined 24 h after infection by Western blot analysis (Fig. 1*B*). Tagged MV-C and Ch proteins were detected in infected cells using anti-Strep-tag antibody and anti-C antibody, thus validating the expression of a second copy of MV-C protein by rMV3/C-STrEP and rMV3/STrEP-C viruses (Fig. 1*B*). Transcription of additional STrEP-C and C-STrEP genes was also controlled by RT-PCR and Sanger sequencing analyses of total RNA extracted from rMV3/C-STrEP and rMV3/STrEP-C–infected cells. We observed that rMV3/C-STrEP was represented by a mixed

recombinant virus population with approximately 60% corresponding to the rMV3/C-STrEP virus and other 40% recombinant MV possessed STOP codon at the beginning of C-STrEP sequence, thus not interfering with STrEP-tag affinity purification. Our polyclonal rMV3/STrEP-C virus-encoded STrEP-C with an additional adenine nucleotide resulting in the mutation of the last C-terminal 14 AA of C protein. Any additional attempts to obtain full-length STrEP-C encoded by MV were unsuccessful. Owing to the numerous problems to rescue perfect recombinant MV expressing additional copy of MV-C protein, we decided to perform our mass spectrometry–based MV-C interactomic analysis on two polyclonal populations of the rMV3/C-STrEP and rMV3/STrEP-C viruses described above and to apply additional conventional approaches to further validate this interactomic analysis.

We assessed the replication efficiency of One-STrEP–tagged MV recombinant viruses by determining single-step growth curves of rMV3/C-STrEP, rMV3/STrEP-C, and rMV3/STrEP-Ch and by comparing them to standard MVSchw. We infected Vero cells with the different One-STrEP–tagged viruses and MVSchw at an MOI 0.1. The growth of recombinant viruses was similar to that of unmodified MVSchw, and titers were comparable (Fig. 1*C*). To further test the potential impact of an additional copy of MV-C gene on viral replication, we compared the infection efficacy of HEK293T, HeLa, and A549 cells by the recombinant viruses at an MOI 1 at 24 h after
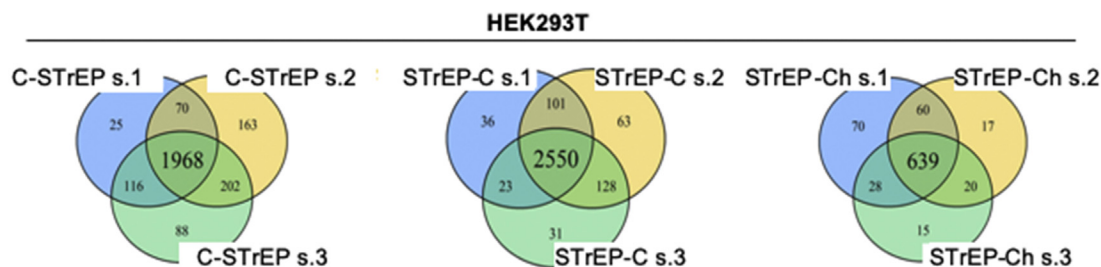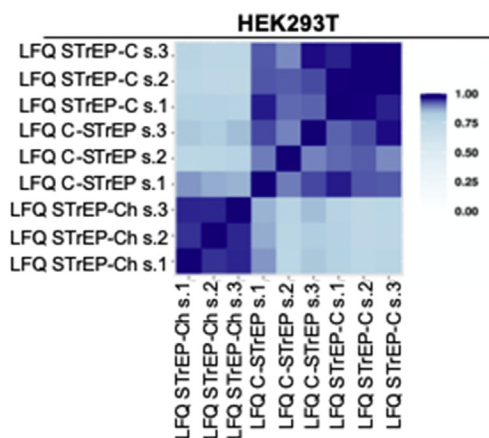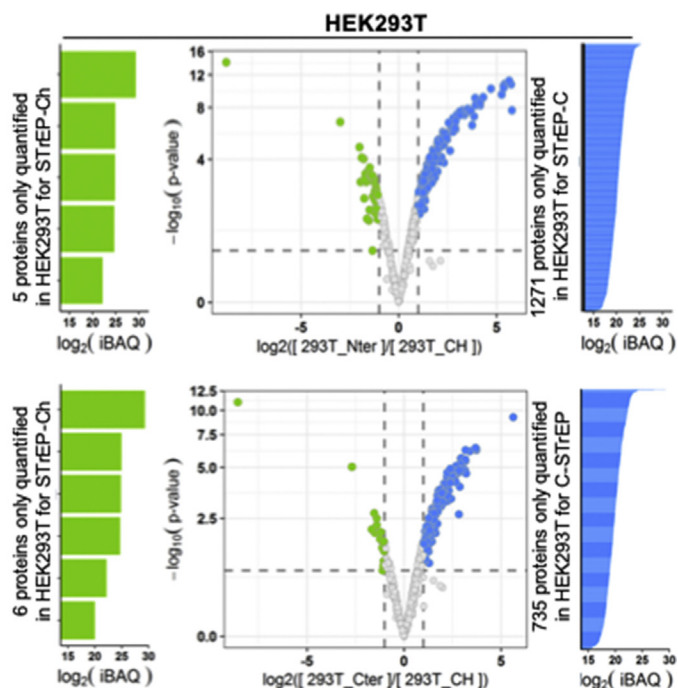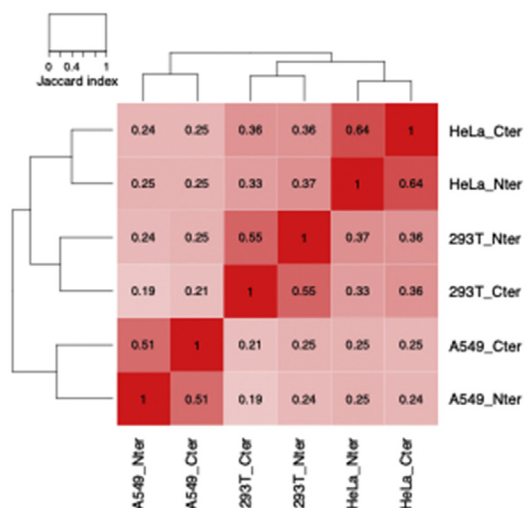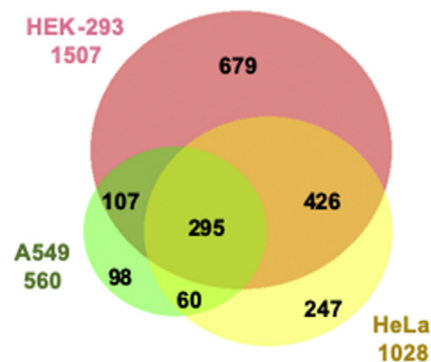
FIG. 3. **Mass spectrometry analysis of MV-C interacting proteins.** *A*, Venn diagrams representing the protein overlap among the three different biological triplicates C-STrEP, STrEP-C, and STrEP-Ch in HEK293 T cells. *B*, correlation matrix obtained for the quality control of the three biological replicates of MV-C Cterm, MV-C Nterm, and Ch conditions in HEK293T cells. *C*, Volcano plots obtained for the comparison of the rMV3/STrEP-Ch and rMV3/STrEP-C, or rMV3/STrEP-Ch and rMV3/C-STrEP conditions in HEK293T cells. *D*, tables show the number of

infection. Immunostaining of MV nucleoprotein and flow cytometry analysis were used to detect infection (Fig. 1D). Replications of rMV3/C-STrEP, rMV3/STrEP-C, and rMV3/STrEP-Ch viruses were comparable in the three cell lines. However, the Western blot analysis of tagged proteins produced by recombinant viruses suggested that more tagged viral proteins were produced in HEK293T than in HeLa and A549 cells (Supplemental Fig. S1). Altogether, recombinant viruses expressing tagged MV-C protein or Ch efficiently propagated in HEK293T, HeLa, and A549 cells.

Identification of Host-Interacting Proteins of MV-C by Affinity Purification and Shotgun Proteomic

To obtain a comprehensive list of direct and indirect interactors of MV-C protein, we applied a previously validated approach based on affinity purification coupled to mass spectrometry analysis of protein cocomplexes (10). To gain a larger spectrum of potential host-interacting proteins of MV-C protein, the analysis was performed on three different cell lines: HEK293T, HeLa, and A549. HEK293 is an extensively validated cell line for high-throughput methods (10, 35, 63–66). A549 and HeLa cells are both human cancer cells: A549 (lung epithelial carcinoma) and HeLa (cervical epithelial adenocarcinoma) are interesting to study, considering the oncolytic activity of MV. The three cell lines were infected with rMV2/STrEP-C and rMV2/C-STrEP at an MOI of 1. Tagged MV-C proteins were purified 24 h after infection by affinity chromatography and copurified cellular proteins (OUTPUT) were directly identified by nano-LC-MS/MS analysis (Fig. 2A). Three independent infections on different days followed by affinity chromatography purification of the MV-C protein cocomplexes were performed for each of the three cell lines. The efficiency of purification was controlled by Western blotting (Fig. 2B). To distinguish between MV-C–associated proteins and nonspecific binding to the beads, coaffinity purification experiments in HEK293T, HeLa, and A549 cells were performed in parallel with the control rMV3/STrEP-Ch virus (Fig. 1A).

To analyze the results, we first filtered reverse proteins and potential contaminant proteins. Raw files were searched using MaxQuant, and the generated protein groups further proceeded with our in-house statistical pipelines to identify the interactors. Our pipeline contains multiple steps for the quality control of the data before the statistical analysis. Figures were generated to illustrate the quality of the data (Fig. 3, A and B and Supplemental Fig. S2, A and B). We found large overlaps between the three biological replicates, demonstrating the robustness of our experimental approach. Further MV-C–specific interacting proteins were determined by applying

additional bioinformatic and statistical analyses (Supplemental Fig. S2C). We kept only proteins with at least 3 quantified LFQ intensity values (LFQ, [52]) in each triplicate/condition. Then, the second filter removed from the original list the proteins that were only present in one condition and not to the other; this means 3 values in one condition only. These proteins were considered as a "present/absent." Present/absent proteins were automatically assigned as significantly enriched in the C-STrEP or STrEP-C condition and are potential MV-C interactors. Then, the remaining proteins were submitted to a differential analysis using a limma t test to compare with the negative control (STrEP-Ch). The corresponding p-values were adjusted using an adaptive Benjamini-Hochberg correction. Differential proteins were plotted in the volcano plot (Fig. 3C and Supplemental Fig. S2, D and E). A cut-off of a fold change of two and FDR threshold of 1% were selected for this experiment to extract the statistically enriched proteins. Finally, together the "present/absent" proteins and differentially enriched proteins resulting from the statistical test were assembled for each MV-C condition to represent the protein of interest (Fig. 3D).

The similarity of proteins captured by MV-C N- and C-terminal tags was studied by calculating Jaccard index between Entrez IDs obtained in the three cell lines. We observed that each cell types clustered together and resulted in 50 to 60% overlap for N-terminal and C-terminal MV-C (Fig. 3E). Owing to this high number of host-interacting proteins common for N- and C-terminally tagged MV-C, the two sets of data for each cell line were assembled together and further compared. Although some cell-specific MV-C interacting proteins were found, more than 50% of captured proteins were shared between the three different cell lines (Fig. 3F). A total of 1507, 1028, and 560 of specific interacting proteins for MV-C protein were specifically captured in HEK293T, HeLa, and A549 cell lines, respectively (Fig. 3F and Supplemental Tables S2 and S3). These important numbers of MV-C interacting proteins represent direct and indirect protein–protein and possibly RNA–protein interactions within the MV-C specific co-complex.

Within this list, some direct interactors of MV-C were previously identified by Y2H, including 26S proteasome regulatory subunit 6A (PSMC3) and WD repeat-containing protein 26 (29). This confirms the sensitivity of our method. In contrast, we failed to identify SHCBP1 interaction with MV-C (29). Preferential localization of SHCBP1 to the nucleus upon infection with the MVSchw in comparison with the minigenome (29) needs to be assessed and might explain the failure to detect MV-C–SHCBP1 complex. Altogether, these data show that our mapping strategy is sensitive and provides reproducible data.

---

identified proteins at each step of the analysis. E, Jaccard matrix showing the similarity of proteins isolated after purification with either C-STrEP or STrEP-C recombinant viruses in three different cell lines. The clustering is unsupervised and groups similar rows/columns together. F, Venn diagram representing final numbers and the overlap in MV-C–specific interacting proteins for HEK293T, HeLa, and A549 cells. MV, measles virus.
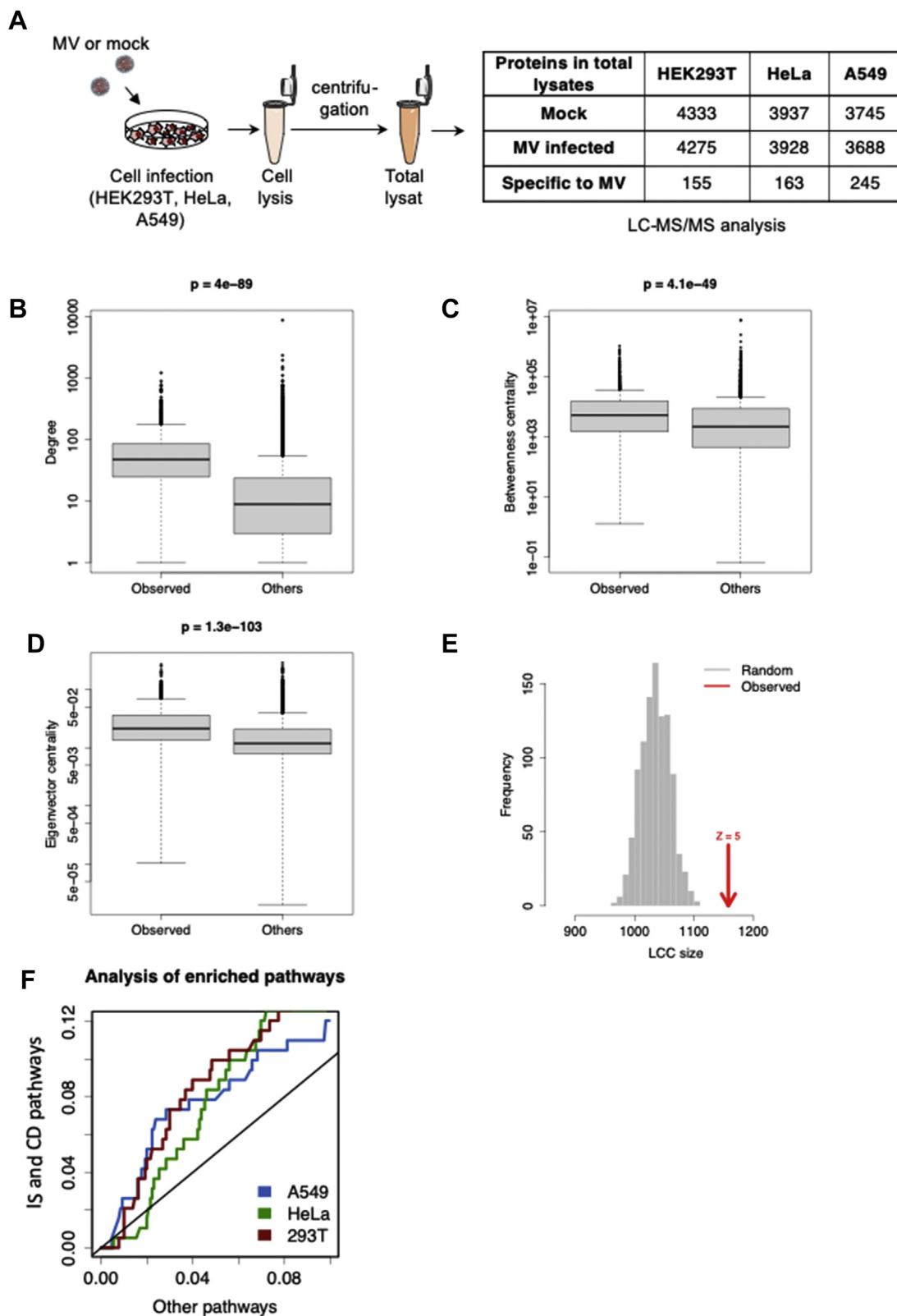

FIG. 4. **Topological analysis and cell pathway enrichment analysis of MV-C interaction network for HEK293T cell line.** *A*, representation of determination of total cell lysates. Cells were either mock-infected or infected with the Schwarz vaccine strain of MV. Twenty-four hours later, the same protocol of purification as in figure 2 was applied. The table shows the number of proteins in the total cell lysate (*B*) degree (*C*)

Topological and Pathway Analysis of MV-C/Host Protein Interaction Network in HEK293T, HeLa, and A549 Cells

We first established a specific list of total proteins separately for HEK293T, HeLa, and A549 cell lines. For this purpose, each cell line under study was either infected or not with MVSchw at an MOI of 1 and lysed 24 h after infection. Total protein lysates (INPUTS) were extracted and subjected to shotgun proteomics (Fig. 4*A*). As described previously, we performed bioinformatic and statistical analyses on total protein data and three cell-specific total protein lists were built, comparing infected with noninfected conditions (Fig. 4*A* and Supplemental Table S4). Because viruses hijack cellular networks by introducing several novel virus–host molecular interactions, understanding viral infection mechanisms is inherently a network problem. Thus, we next analyzed MV-C protein interaction networks individually in HEK293T, A549, or HeLa cell lines for specific topological features using several standard network centrality measures (67). We first asked whether host proteins that copurified with MV-C are central in the human interactome network (68). Local (degree) and global (betweenness) centrality measures were calculated. The degree of a protein in a network corresponds to its number of direct partners and is, therefore, a measure of local importance. Betweenness is a global measure of centrality, as it measures the number of shortest paths (the smallest distances between any two proteins in the network) that go through a given protein. The degree distribution of cellular proteins copurified with MV-C was plotted and compared with the distribution obtained for the rest of the human interactome network of each cell type (Fig. 4*B*, Supplemental Figs. S3*A* and S4*A*). These distributions were significantly distinct (p-value $< 4e \times 10^{-89}$ under a Mann–Whitney test for HEK293T). Thus, the cellular proteins that copurified with MV-C exhibit much more cellular partners than normally expected by chance. We also calculated and plotted the betweenness centrality distribution for the cellular proteins that copurified with MV-C (Fig. 4*C*, Supplemental Figs. S3*B* and S4*B*). This distribution was significantly different from the one obtained for the rest of human interactome network of each cell type (p-value $< 4.1 \times 10^{-49}$ for HEK293T). Thus, betweenness centrality measures show that MV-C interacting partners are enriched for proteins that connect multiple regions in the human interactome. Furthermore, we measured the eigenvector centrality of MV-C host-interacting proteins. This approach measures the influence of a node in a network. Relative scores are assigned to all nodes in the network based on the concept

that connections to high-scoring nodes contribute more to the score of the node in question than equal connections to low-scoring nodes. For MV-C protein network, the observed nodes were connected to many nodes that had high scores (Fig. 4*D*, Supplemental Figs. S3*C* and S4*C*). Betweenness and eigenvector centrality measures were shown to be highly correlated with Pearson correlation coefficients ranging between 0.82 and 0.91. Hence, our network centrality metrics supported the fact that MV-C interacting proteins are more central in the human interactome and come in support of the idea that they might play an important role in cellular processes.

Furthermore, we explored whether MV-C interacting proteins were forming cohesive subgraphs, as is generally observed for "disease modules" (61). For this, we computed the size of the largest connected component (LCC) of the subgraph formed by the MV-C host-interacting proteins. We then selected the same number of proteins at random in the interactome and computed the size of the LCC, repeating the process 1000 times. Finally, we computed a Z-score to quantify the significance of the observed value, corresponding to the number of SDs that the observed value departed from the expected value of the random distribution. We found for HEK293T a Z-score of 5 (N = 1158 of 1498 proteins in the LCC, compare with 1045 ± 23 expected at random), showing that MV-C proteins form a cohesive disease module (Fig. 4*E*, Supplemental Figs. S3*D* and S4*D*).

Next, we looked for functional differences between MV-C–specific interacting proteins in the three cell lines. We performed a pathway enrichment analysis for MV-C–specific interacting proteins in HEK293T, HeLa, and A549 cell lines (Supplemental Fig. S5). This was performed using Kyoto Encyclopedia of Genes and Genomes pathway analysis *via* the DAVID database. We observed that MV-C interactors were enriched in spliceosome, ribosome, and protein processing in the endoplasmic reticulum, proteasome, oxidative phosphorylation, Huntington's disease, and Epstein-Barr virus infection pathways. Of note, no cancer cell–specific signature for HeLa and A549 in comparison with the HEK293T cell line was observed. We obtained a longer list of pathways enriched in HEK293T cells that was likely due to the higher number of MV-C–specific interactors than HeLa and A549 (Fig. 3*F* and Supplemental Tables S2 and S3). This can be explained by a better expression of tagged MV-C in HEK293T than in HeLa and A549 cells (Supplemental Fig. S1). To further address the cell-specific analysis of MV-C interacting proteins, we extracted a list of highest degree nodes in the interactome for

---

betweenness (*D*) eigenvector centrality distributions of MV-C interaction partners and proteins from the rest of the interactome in HEK293T cell line. Others correspond to detectable in HEK293T cell line proteins from (*A*). *E*, distribution of sizes of the largest connected component (LCC) of random sets of proteins with the same number as MV-C interaction partners in the interactome of HEK293T. The *arrow* shows the observed LCC for MV-C. *F*, ROC curves showing the enrichment in the immune system (IS) and cell death (CD) pathways (overall pathways) in HEK293T, HeLa, and A549 cells (see Supplemental Table S6). *Curves* above the *diagonal* indicate enrichment in true positive pathways (IS and SD). MV, measles virus; ROC, receiver operating characteristic.
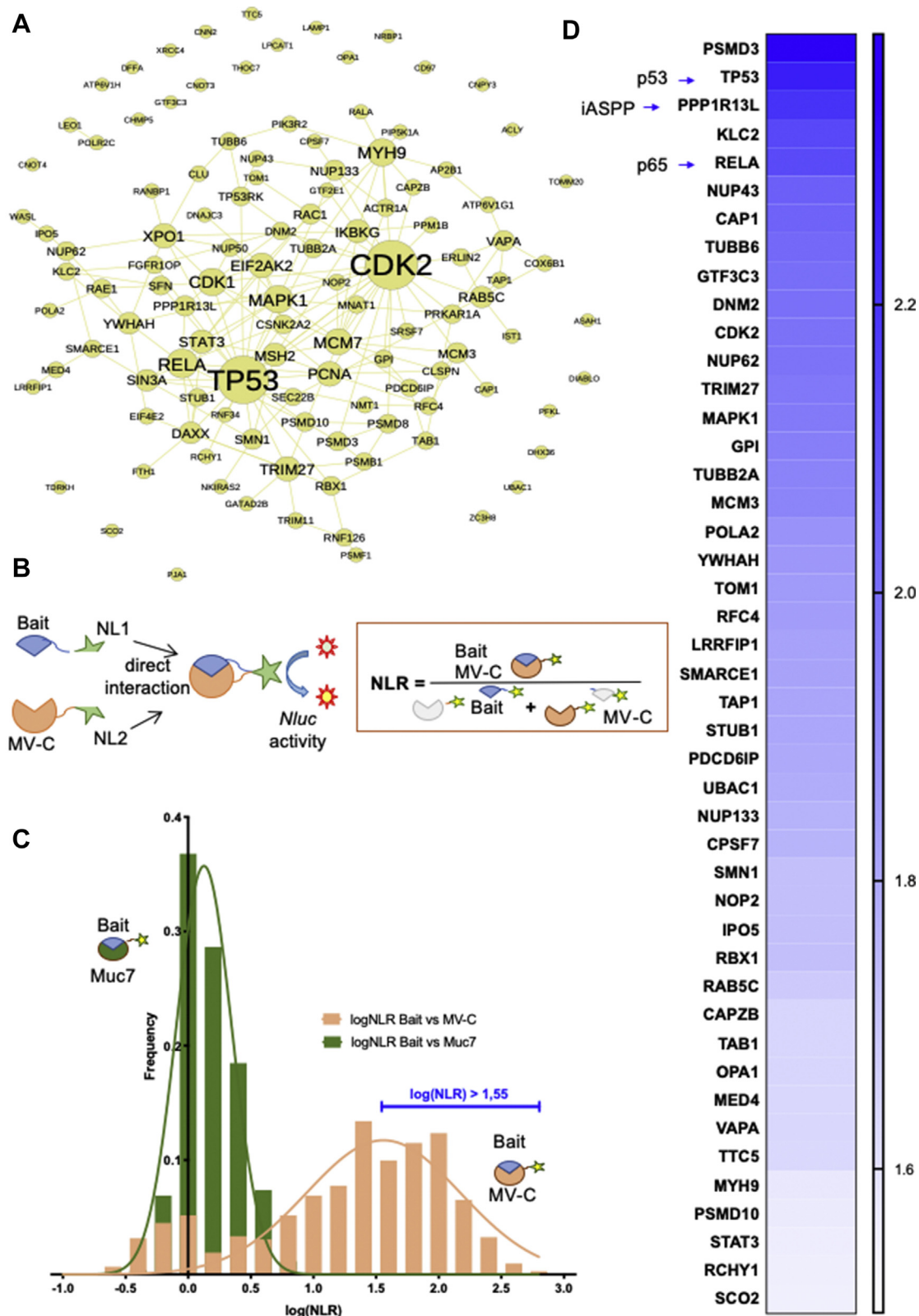
Fig. 5. **Protein complementation assay (PCA) for MV-C protein and 119 host-interacting proteins.** *A*, representation of the PPI network selected for PCA. Gephi 0.9.2 was used to represent the PPI network. *B*, schematic representation of PCA approach. A host protein (prey) is fused downstream to the N-half of the Nluc (NL1). MV-C (bait) is fused downstream to the C-half of the Nluc (NL2). The formula to calculate normalized luminescence ratio (NLR) for a given protein pair is shown. *C*, frequency distribution of log(NLR) values for the MV-C and the Muc7

each cell type (Supplemental Table S5). Several known cellular high degree nodes such as YWHAQ, YWHAZ, YWHAH, YWHAG, YWHAE, CDK1, CDK2, PRKACA, PPP1CA, HSP90AB1, and HSP90AA1 were observed and represented proteins implicated in the regulation of a large spectrum of both general and specialized signaling pathways. Interestingly, MAPK1, RELA, and EIF2AK2 were observed in the highest degree node list for HEK293T, HeLa and A549; these proteins are part of more specialized signaling pathways related to immune response and cell death.

We tested the hypothesis that the two major cellular pathways which are Immune System and Cell Death pathways (overall referred to as IS and CD) were specifically enriched in the MV-C network for the three cell types (Supplemental Tables S6–S9). For this, we performed a pathway enrichment analysis on MV-C–specific networks in the three different cell lines. Similarly to the topological analysis, the total protein data set was used as a background for all pathways and disease gene enrichments (Fig. 4A and Supplemental Table S3). Pathways were taken from MSigDB v3.1 (69) and Wikipathways (70), with a total of 8690 sets of genes. For each pathway, the significance of its overlap with MV-C partners was assessed by computing a hypergeometric *p*-value, with a background set to be the total protein data set for each cell line. To test that IS and CD pathways were overrepresented in the most enriched pathways, we computed a receiver operating characteristic curve for each cell type (Fig. 4F). We ranked pathways according to their *p*-value, from the lowest to highest. We then plotted the receiver operating characteristic curves, showing the enrichment in IS and CD pathways (*y* axis, true-positive rate) in the top of the list compared with other pathways (*x* axis, false-positive rate) and showed the enrichment for the three cell types (Fig. 4F). Altogether, topological analyses of the MV-C interaction network demonstrate that MV-C preferentially interacts, either directly or indirectly, with host proteins that are central in the human interactome network. MV-C protein co-complexes represent well-defined functional modules as assessed by the enrichment for proteins sharing interactions. This is clearly in line with the proposed role of MV-C in the regulation of innate immune response and cell death pathways.

PCA to Study MV-C Direct Interacting Proteins Involved in Immune Response and Cell Death Pathways

Based on the results of IS and CD pathway enrichment analysis (Fig. 4F), hypothesis-driven selection of 119 MV-C–specific interacting proteins was conducted (Supplemental Table S1). In the human proteome, these proteins are connected to each other in a PPI network where TP53 (p53) and

CDK2 play the role of hubs increasing connectivity between the MV-C and cellular targets (Fig. 5A). To further specify PPIs between MV-C and the selected host-interacting proteins involved in cell death, immune response, and infectious disease pathways, we applied a PCA based on the split luciferase (71). We used a modified version of the PCA approach assigned NlucPCA for Nanoluc luciferase PCA (N2H, [43]). In NlucPCA, the luciferase activity is restored leading to luminescence signal when the two fragments of the Nluc are in close contact (10 nm), resulting from the direct PPI between the prey and the bait fused to Nluc luciferase fragments 1 and 2 (NL1 and NL2), respectively (Fig. 5B). Hundred and nineteen potential interactors (Supplemental Table S1) were screened against MV-C. These 119 host proteins were also screened against an unrelated Muc7 protein as a negative control to determine the cut-off of nonspecific binding. The Gaussian repartition of the NLR of Muc7 and MV-C gave us a threshold of two SDs at an log(NLR) of 1.55 that was applied to filter the positive interactors (Fig. 5C). From the list of 119 MV-C–specific interacting proteins, we validated the direct interaction with MV-C for 45 host proteins (Fig. 5D). Thus, PCA provided additional validation to the sensitivity and specificity of our mass spectrometry approach and further narrowed the list of specific MV-C protein network to its direct PPIs.

BRET Method Confirms MV-C Direct PPIs With iASPP and p65

We found high NlucPCA scores for p53, iASPP, and p65 (Fig. 5D) and further addressed their direct interactions with MV-C. None of the selected proteins (p53, iASPP, and p65) have previously been described as a direct partner of MV-C.

To study MV-C PPIs directly in live cells with simultaneous control of protein-expression efficacy, we applied the BRET approach. With this aim, iASPP, p53, and p65 were fused with YFP coding sequence, and MV-C was tagged with Nluc, either N-terminal or C-terminal (Fig. 6A). BRET signals indicating MV-C interaction with iASPP, p53, or p65 were measured in living cells 48 h after transfection of plasmids expressing YFP- and Nluc-tagged proteins at different concentration ratios of DNA. As positive and negative controls, we used EYFP fused to Nluc and superoxide dismutase 1 (SOD1) fused with the Nluc C-terminally, respectively. For each protein pair, we calculated the NetBret that represents the direct bioluminescence from the donor (Nluc) and the acceptor (NlucY) normalized to the SOD1-Nluc control (Fig. 6, B and C). We observed that for every studied protein, the netBret value increased while the expression of the donor increased (Fig. 6C) and thus the ratio MV-C:interactor decreased. The NetBret values were similar for MV-C–tagged C- or

---

with corresponding superimposed fitted Gaussian curves. For the MV-C PCA, each protein pair was assessed in three biological replicates and for Muc7 in two biological replicates. The threshold of two SDs corresponding to the log(NLR) of 1.55 was applied based on Gaussian repartition of the log(NLR) of Muc7 and MV-C. *D*, the list of 45 MV-C protein interactors validated by PCA. MV, measles virus; Nluc, nanoluciferase; PPI, protein–protein interaction.
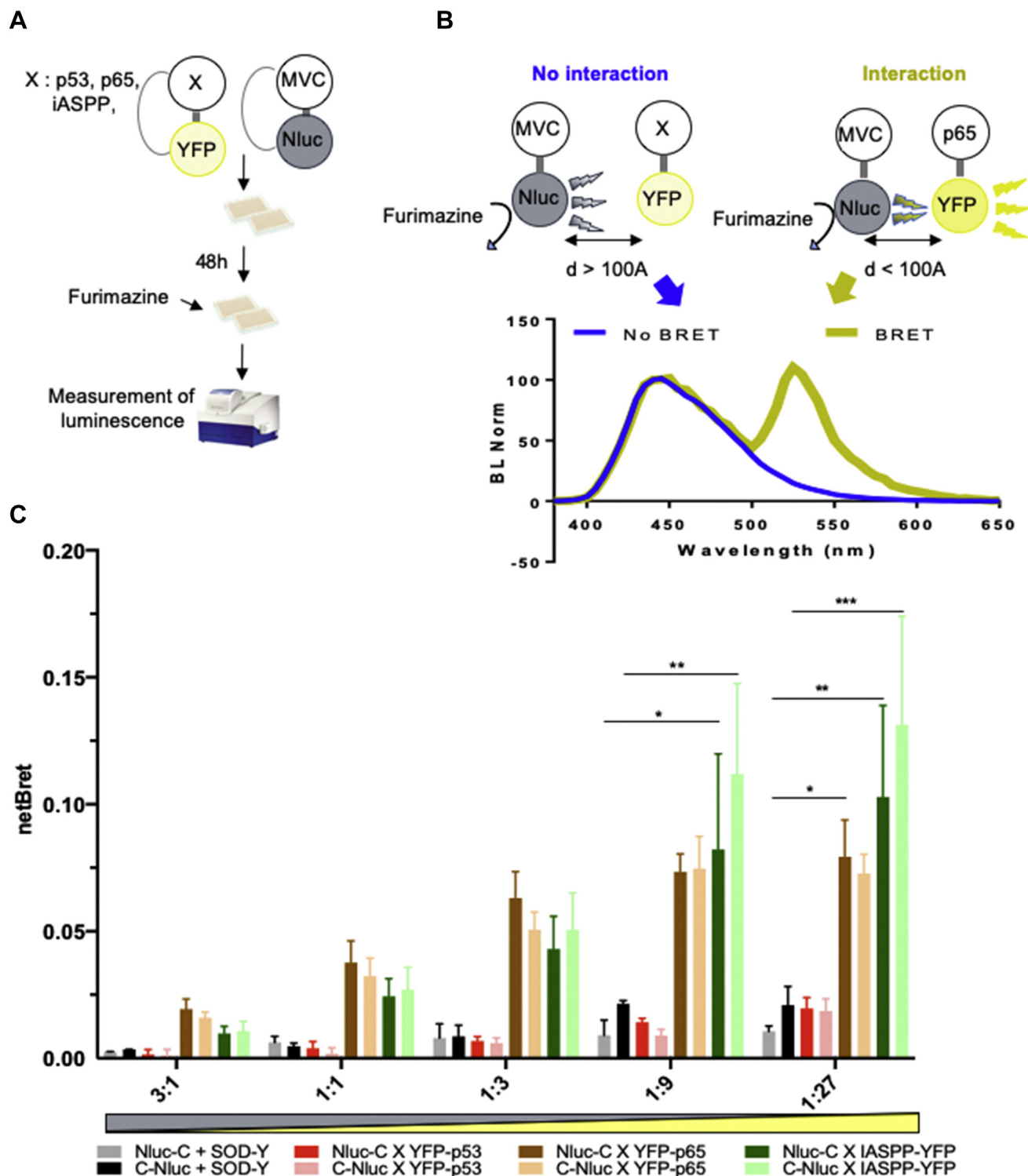
FIG. 6. **BRET analysis of MV-C direct interactions with iASPP, p65, or p53.** *A*, the BRET method applied to study interactions between MV-C and iASPP, p65, or p53. HEK293T cells were transfected for 48 h with two plasmids expressing YFP- and Nluc-tagged proteins in N- and C-terminal positions at five DNA ratios, from 3:1 to 1:27. BRET was measured, and 20 min later, furimazine was added. The donor signal (Nluc, 448.5–472.5 nm emission) and acceptor signal (NlucY, 522.5–547.5 nm emission) were measured using a bioluminescence plate reader. *B*, the molecular principle of the BRET assay. The donor, Nluc, oxidizes furimazine substrate into furimamide emitting light around 460 nm. When BRET pair–tagged proteins directly interact, the proximity of Nluc will excite YFP, which in turn emits a yellow light around 530 nm. If there is no interaction, no yellow emission will occur. *C*, assessment of MV-C PPI with iASPP, p65, or p53. Each value is the mean of all the combinations

N-terminally with the Nluc. Thus, similar to tagged protein affinity purification results (Fig. 3E), the interaction was not influenced by the tag and both N- and C-terminal–tagged MV-C interacted at the same level. MV-C protein interactions with iASPP and p65 presented a significantly high value of netBret, whereas MV-C interaction with p53 demonstrated low values. Thus, we failed to validate p53 direct PPI with MV-C by BRET (Fig. 6C). However, we kept p53 protein for further functional studies as a failure in a single PPI assay does not completely exclude the direct PPI observed by the PCA approach.

Functional Analysis of iASPP, p65, and 53 Roles in MV Replication

We first infected HeLa or HEK293T cells with recombinant viruses expressing tagged MV-C to validate by affinity chromatography purification coupled to Western blot analysis PPIs of MV-C with p65, iASPP, and p53 during infection (Fig. 7A).

We then investigated the functional roles of IASPP, p65, and p53 in MV replication. We used HEK293T cells to generate additional cell lines with targeted deletion of *PPP1R13L* (iASPP), *RelA* (p65), and *TP53*(p53). We validated the KO HEK293T cells by Western blot (Fig. 7B). Then we assessed the replication efficiency of MVSchw by determining viral growth curves. There was no effect on MV replication with p65 expression absent, whereas MV replication was almost completely blocked in iASPP KO and p53 KO cells compared with control (Ctrl) HEK293T cells (Fig. 7C, top panel). In the same experiment, we tested the replication of rMVΔC available in our laboratory, which is deficient in C protein expression (32). Linear regression models with three factors (time, p65, or Ctrl, MV or MVΔC) were estimated to compare MVSchw and rMVΔC viruses' replication in Ctrl and p65 KO cell lines (Fig. 7C, bottom panel). Student t tests were used to test the nullity of coefficients related to each factor. Considering all time points, the coefficient related to MV/MVΔC is significantly not null ($p = 8.50e-05$), which shows a significant difference of the virus growth in p65–/– and Ctrl cells, whereas the coefficient related to p65/Ctrl is less significantly nonzero ($p = 0.13$). Next, we compared the time dynamics of virus growth for MV and MVΔC cells from 36 h after infection by estimating linear regression models with interactions between the time and the p65/Ctrl factor. Quite interestingly, we found no significant effect for the time, the p65/Ctrl factor, and their interaction for MV-infected cells, whereas we found significant effects for all model parameters for MVΔC-infected cells: p-values corresponding to the test of the nullity of the interaction factor between the time and p65/Ctrl are displayed on the

graph. It shows that the time dynamics of virus growth is significantly different for p65 MVΔC cells from 36 h after infection than for Ctrl MVΔC cells. More precisely, MVΔC growth is decreasing with time in Ctrl cells, whereas it remains constant in p65 KO cells on this time range (Fig. 7C, bottom panel). No rescuing of rMVΔC replication was observed in iASPP KO and p53 KO cells (data not shown). Thus, our functional experiments with iASPP KO and p53 KO cells suggest an essential role of these two proteins on MV replication and a negative role of p65 protein on rMVΔC replication that is no longer observed when MV-C is present.

DISCUSSION

This study aimed to establish the MV-C protein network of interactions in MV-infected cells. We used a strategy based on recombinant viruses expressing tagged viral proteins followed by affinity purification and a bottom-up mass spectrometry–based proteomics (10). This proteomic approach allowed us to obtain a list of MV-C–specific host partners interacting *via* direct or indirect PPIs. In addition, the high number of positively scored MV-C interacting proteins could also be explained by RNA–protein interactions, as our affinity chromatography purification protocol did not include a nuclease digestion step. By performing topological and signaling pathway–oriented analyses of MV-C host-interacting proteins, we observed that MV-C was embedded in a complex host interactome. Of note, we observed an enrichment for RNA-associated processes that further indicate a role for RNA–protein interactions within the MV-C–specific complex. In the future, additional affinity purifications in the presence of nucleases such as RNases should be performed to separate MV-C–specific protein–protein and RNA–protein interactions. Advanced computational tools recently developed in network biology highlighted the immunity and cell death pathways as specifically enriched in the MV-C network for the three cell types tested: HEK293T, HeLa, and A549 (Fig. 4F). Furthermore, we mainly focused on these two cell pathways (immune system and cell death), as MV vaccine and modified recombinant MV strains are of high application in vaccinology and in cancer treatment.

To validate and to specify PPIs found by our MS approach, we applied two unbiased approaches to study PPIs: PCA based on the split luciferase and BRET. PCA allowed us to validate that from a list of 119 host proteins that form a specific protein co-complex with MV-C upon infection and belong to cell death, immune response, and infectious disease pathways, 45 proteins were likely direct interactors (Fig. 5D).

between Nluc-tagged host proteins and YFP-tagged viral proteins of each protein. netBret represents the acceptor/donor ratio by dividing the initial fluorescence measurements (530 nm) by the luminescence measurements (485 nm) and subtracting out background luminescence (BRET readings in cells expressing the donor without any acceptor). The *gray* and *yellow triangles*, respectively, correspond to the concentration of acceptor and donor plasmids that varies according to the plasmid ratio. Error bars represent ±SEM of four biological replicates. Statistical significance for each protein pair was determined by two-way ANOVA (*$p < 0.05$, **$p < 0.01$, ***$p < 0.001$). BRET, bioluminescence resonance energy transfer; PPI, protein–protein interaction; Nluc, nanoluciferase; SOD1, superoxide dismutase 1.
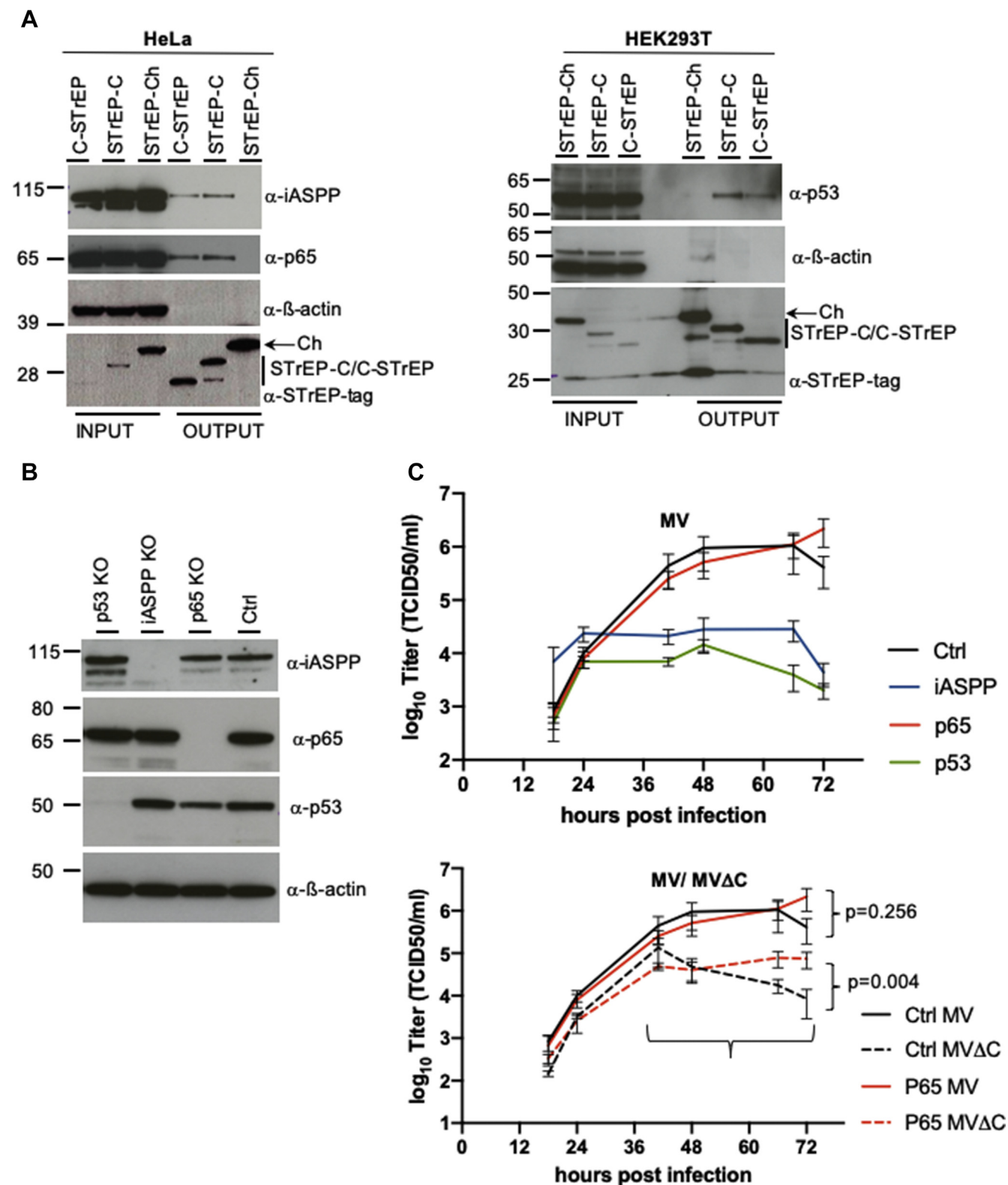
A

B

C

FIG. 7. **Role of iASPP, p65, and 53 in MV replication.** *A*, validation of MV-C binding with p65 and iASPP in infected cells. HeLa (*left panel*) or HEK293T (*right panel*) cells were infected with rMV3/C-STrEP, rMV3/STrEP-Ch, or rMV3/STrEP-C. Total lysates (INPUT) and MV-C–specific protein complexes (OUTPUT) were analyzed by Western blot using p65, iASPP, and p53 and One-STrEP-tag antibodies. Western blot analysis of β-actin served as a control for loading and for nonspecific binding. Western blot shows one representative experiment of two biological

However, we cannot totally exclude that some detected pairs were indirect interacting proteins. Thus, the PCA provided additional validation to the sensitivity and specificity of our mass spectrometry approach and further narrowed the MV-C protein network to its direct PPIs.

p53, iASPP, and p65 were three host factors that drew our attention as they possessed the highest luciferase scores in PCA (Fig. 5C). Their interactions with MV-C were further studied by BRET approach. None of these proteins (p65, p53, and iASPP) has previously been described as a direct partner of MV-C. p65, p53 and iASPP proteins interact with each other. Indeed, iASPP inhibits p53-mediated apoptosis (72, 73) and binds RelA/p65 to inhibit its transcriptional activity (74, 75). These two binding partners of iASPP explain why under certain conditions iASPP may have proapoptotic and anti-apoptotic effects, depending on iASPP regulation of p53 or RelA/p65, respectively. High netBret values confirmed MV-C protein interactions with iASPP and p65 (Fig. 6C). However, we failed to validate MV-C interaction with p53 by BRET analysis. Indeed, p53 demonstrated low netBret values that were comparable with the negative control (SOD1). As no single PPI assay is exceptionally superior to any other, additional PPI approaches should be applied to further examine the possibility of direct PPI between p53 and MV-C. In addition, we validated MV-C specific PPI with iASPP, p53, and RelA/p65 in infected cells (Fig. 7A). Thus, iASPP, p53, and RelA/p65 proteins are in complex with MV-C in MV-infected cells.

To further demonstrate the functional relevance of the PPIs found for MV-C, we generated iASPP KO, p53 KO, and p65 KO cells and assed MV replication. Depletion of iASPP and p53 proteins led to almost complete abrogation of viral replication in the corresponding KO cells, suggesting an essential role of these two host proteins on MV replication. In p65 KO cells, MVSchw virus replicated as efficiently as in the control cell line (Fig. 7C, top panel). We next assessed replication of rMVΔC in p65 KO and Ctrl cells. Significant reduction of rMVΔC replication was observed in Ctrl and p65 KO cells. This could be explained by the previously described accumulation of DI RNA genomes in cells infected by rMVΔC (21, 32). In addition, the suggested role of MV-C protein in control of the cell apoptosis could also explain the observed difference in MVSchw and rMVΔC replication (23, 38). Importantly, when rMVΔC was assessed in p65 KO cells, its replication was partially rescued (Fig. 7C, bottom panel). This result implies the key positive role of the direct p65-MV-C PPI interaction on MV replication. Previous studies suggested that MV-V binding to p65 could suppress NF-κB promoter activity (76). For MV,

both virulence factors MV-V and MC-C interact with the same host proteins (p53 and p65). We believe that this multiple targeting of the same host protein contributes synergistically to the control of the same cellular pathway. However, future studies should depicture detailed molecular mechanisms that are behind MV-C binding to p65.

Viral virulence factors are embedded into a complex host interactome, enabling the virus to control the host cell to provide efficient viral replication. MV-C is such an example. We applied various PPI approaches that allowed us to glimpse the interplay of the dual-functional role of MV-C in controlling both cell death and host innate immune responses. We believe that our results provide first solid support for further studies that will focus on precise molecular mechanisms by which MV-C controls the host cells.

replicates. B, Western blot analysis to validate efficient KO of iASPP, p65, and p53 expression in HEK293T cells. Western blot shows one representative experiment of two biological replicates. C, virus growth curves obtained for MV Schwarz (*top panel*) or MV Schwarz and MVΔC (*bottom panel*). HEK293T Ctrl, p65–/–, iASPP–/–, or p53–/– cells were infected with MV Schwarz or MVΔC at an MOI of 0.05. Cell-associated virions were recovered at each time point, and titers were determined using the TCID50 method. Each point represents the mean and 95% confidence interval of values obtained from four biological replicates. MOI, multiplicity of infection; MV, measles virus.

performed MS data analysis. M. S. and I. A. K. performed topological and pathway analyses. Y. J. helped with the protein fragment complementation assay and R. G. with bioluminescence resonance energy transfer analyses. A. V. K. wrote the article, whereas all authors endorse its content.

REFERENCES

1. Frantz, P. N., Teeravechyan, S., and Tangy, F. (2018) Measles-derived vaccines to prevent emerging viral diseases. *Microbes Infect.* **20**, 493–500
2. Russell, S. J., Babovic-Vuksanovic, D., Bexon, A., Cattaneo, R., Dingli, D., Dispenzieri, A., Deyle, D. R., Federspiel, M. J., Fielding, A., Galanis, E., Lacy, M. Q., Leibovich, B. C., Liu, M. C., Munoz-Alia, M., Miest, T. C., *et al.* (2019) Oncolytic measles virotherapy and opposition to measles vaccination. *Mayo Clin. Proc.* **94**, 1834–1839
3. Cattaneo, R., Kaelin, K., Baczko, K., and Billeter, M. A. (1989) Measles virus editing provides an additional cysteine-rich protein. *Cell* **56**, 759–764
4. Bellini, W. J., Englund, G., Rozenblatt, S., Arnheiter, H., and Richardson, C. D. (1985) Measles virus P gene codes for two proteins. *J. Virol.* **53**, 908–919
5. Caignard, G., Guerbois, M., Labernardiere, J. L., Jacob, Y., Jones, L. M., Wild, F., Tangy, F., and Vidalain, P. O. (2007) Measles virus V protein blocks Jak1-mediated phosphorylation of STAT1 to escape IFN-alpha/beta signaling. *Virology* **368**, 351–362
6. Caignard, G., Komarova, A. V., Bourai, M., Mourez, T., Jacob, Y., Jones, L. M., Rozenberg, F., Vabret, A., Freymuth, F., Tangy, F., and Vidalain, P. O. (2009) Differential regulation of type I interferon and epidermal growth factor pathways by a human Respirovirus virulence factor. *PLos Pathog.* **5**, e1000587
7. Jiang, Y., Qin, Y., and Chen, M. (2016) Host-pathogen interactions in measles virus replication and anti-viral immunity. *Viruses* **8**, 308
8. Mandhana, R., Qian, L. K., and Horvath, C. M. (2018) Constitutively active MDA5 proteins are inhibited by paramyxovirus V proteins. *J. Interferon Cytokine Res.* **38**, 319–332
9. Cruz, C. D., Palosaari, H., Parisien, J. P., Devaux, P., Cattaneo, R., Ouchi, T., and Horvath, C. M. (2006) Measles virus V protein inhibits p53 family member p73. *J. Virol.* **80**, 5644–5650
10. Komarova, A. V., Combredet, C., Meyniel-Schicklin, L., Chapelle, M., Caignard, G., Camadro, J. M., Lotteau, V., Vidalain, P. O., and Tangy, F. (2011) Proteomic analysis of virus-host interactions in an infectious context using recombinant viruses. *Mol. Cell Proteomics* **10**. M110 007443
11. Sanchez-Aparicio, M. T., Feinman, L. J., Garcia-Sastre, A., and Shaw, M. L. (2018) Paramyxovirus V proteins interact with the RIG-I/TRIM25 regulatory complex and inhibit RIG-I signaling. *J. Virol.* **92**, e01960-17
12. Nagai, Y., and Kato, A. (2004) Accessory genes of the paramyxoviridae, a large family of nonsegmented negative-strand RNA viruses, as a focus of active investigation by reverse genetics. *Curr. Top. Microbiol. Immunol.* **283**, 197–248
13. Alkhatib, G., Massie, B., and Briedis, D. J. (1988) Expression of bicistronic measles virus P/C mRNA by using hybrid adenoviruses: Levels of C protein synthesized *in vivo* are unaffected by the presence or absence of the upstream P initiator codon. *J. Virol.* **62**, 4059–4069
14. Nishie, T., Nagata, K., and Takeuchi, K. (2007) The C protein of wild-type measles virus has the ability to shuttle between the nucleus and the cytoplasm. *Microbes Infect* **9**, 344–354
15. Devaux, P., Hodge, G., McChesney, M. B., and Cattaneo, R. (2008) Attenuation of V- or C-defective measles viruses: Infection control by the inflammatory and interferon responses of rhesus monkeys. *J. Virol.* **82**, 5359–5367
16. Escoffier, C., Manie, S., Vincent, S., Muller, C. P., Billeter, M., and Gerlier, D. (1999) Nonstructural C protein is required for efficient measles virus replication in human peripheral blood cells. *J. Virol.* **73**, 1695–1698
17. McAllister, C. S., and Samuel, C. E. (2009) The RNA-activated protein kinase enhances the induction of interferon-beta and apoptosis mediated by cytoplasmic RNA sensors. *J. Biol. Chem.* **284**, 1644–1651
18. Mrkic, B., Odermatt, B., Klein, M. A., Billeter, M. A., Pavlovic, J., and Cattaneo, R. (2000) Lymphatic dissemination and comparative pathology of recombinant measles viruses in genetically modified mice. *J. Virol.* **74**, 1364–1372
19. Nakatsu, Y., Takeda, M., Ohno, S., Koga, R., and Yanagi, Y. (2006) Translational inhibition and increased interferon induction in cells infected with C protein-deficient measles virus. *J. Virol.* **80**, 11861–11867
20. Patterson, J. B., Thomas, D., Lewicki, H., Billeter, M. A., and Oldstone, M. B. (2000) V and C proteins of measles virus function as virulence factors in vivo. *Virology* **267**, 80–89
21. Pfaller, C. K., Mastorakos, G. M., Matchett, W. E., Ma, X., Samuel, C. E., and Cattaneo, R. (2015) Measles virus defective interfering RNAs are generated frequently and early in the absence of C protein and can be destabilized by adenosine deaminase acting on RNA-1-like hypermutations. *J. Virol.* **89**, 7735–7747
22. Pfaller, C. K., Radeke, M. J., Cattaneo, R., and Samuel, C. E. (2014) Measles virus C protein impairs production of defective copyback double-stranded viral RNA and activation of protein kinase R. *J. Virol.* **88**, 456–468
23. Richetta, C., Gregoire, I. P., Verlhac, P., Azocar, O., Baguet, J., Flacher, M., Tangy, F., Rabourdin-Combe, C., and Faure, M. (2013) Sustained autophagy contributes to measles virus infectivity. *PLoS Pathog.* **9**, e1003599
24. Takeuchi, K., Takeda, M., Miyajima, N., Ami, Y., Nagata, N., Suzaki, Y., Shahnewaz, J., Kadota, S., and Nagata, K. (2005) Stringent requirement for the C protein of wild-type measles virus for growth both in vitro and in macaques. *J. Virol.* **79**, 7838–7844
25. Fontana, J. M., Bankamp, B., Bellini, W. J., and Rota, P. A. (2008) Regulation of interferon signaling by the C and V proteins from attenuated and wild-type strains of measles virus. *Virology* **374**, 71–81
26. Shaffer, J. A., Bellini, W. J., and Rota, P. A. (2003) The C protein of measles virus inhibits the type I interferon response. *Virology* **315**, 389–397
27. Yokota, S., Okabayashi, T., and Fujii, N. (2011) Measles virus C protein suppresses gamma-activated factor formation and virus-induced cell growth arrest. *Virology* **414**, 74–82
28. Sparrer, K. M., Pfaller, C. K., and Conzelmann, K. K. (2012) Measles virus C protein interferes with Beta interferon transcription in the nucleus. *J. Virol.* **86**, 796–805
29. Ito, M., Iwasaki, M., Takeda, M., Nakamura, T., Yanagi, Y., and Ohno, S. (2013) Measles virus nonstructural C protein modulates viral RNA polymerase activity by interacting with host protein SHCBP1. *J. Virol.* **87**, 9633–9642
30. Nakatsu, Y., Takeda, M., Ohno, S., Shirogane, Y., Iwasaki, M., and Yanagi, Y. (2008) Measles virus circumvents the host interferon response by different actions of the C and V proteins. *J. Virol.* **82**, 8296–8306
31. Pfaller, C. K., Bloyet, L. M., Donohue, R. C., Huff, A. L., Bartemes, W. P., Yousaf, I., Urzua, E., Claviere, M., Zachary, M., de Masson d'Autume, V., Carson, S., Schieferecke, A. J., Meyer, A. J., Gerlier, D., and Cattaneo, R. (2019) The C protein is recruited to measles virus ribonucleocapsids by the phosphoprotein. *J. Virol.*, e01733-19

32. Mura, M., Combredet, C., Najburg, V., Sanchez David, R. Y., Tangy, F., and Komarova, A. V. (2017) Non-encapsidated 5' copy-back defective-interfering genomes produced by recombinant measles viruses are recognized by RIG-I and LGP2 but not MDA5. *J. Virol.*, e00643-17

33. McAllister, C. S., Toth, A. M., Zhang, P., Devaux, P., Cattaneo, R., and Samuel, C. E. (2010) Mechanisms of protein kinase PKR-mediated amplification of beta interferon induction by C protein-deficient measles virus. *J. Virol.* **84**, 380–386

34. Runge, S., Sparrer, K. M., Lassig, C., Hembach, K., Baum, A., Garcia-Sastre, A., Soding, J., Conzelmann, K. K., and Hopfner, K. P. (2014) In vivo ligands of MDA5 and RIG-I in measles virus-infected cells. *PLoS Pathog.* **10**, e1004081

35. Sanchez David, R. Y., Combredet, C., Sismeiro, O., Dillies, M. A., Jagla, B., Coppee, J. Y., Mura, M., Guerbois Galla, M., Despres, P., Tangy, F., and Komarova, A. V. (2016) Comparative analysis of viral RNA signatures on different RIG-I-like receptors. *Elife* **5**, e11275

36. Hur, S. (2019) Double-Stranded RNA sensors and modulators in innate immunity. *Annu. Rev. Immunol.* **37**, 349–375

37. Xia, M., Gonzalez, P., Li, C., Meng, G., Jiang, A., Wang, H., Gao, Q., Debatin, K. M., Beltinger, C., and Wei, J. (2014) Mitophagy enhances oncolytic measles virus replication by mitigating DDX58/RIG-I-like receptor signaling. *J. Virol.* **88**, 5152–5164

38. Toth, A. M., Devaux, P., Cattaneo, R., and Samuel, C. E. (2009) Protein kinase PKR mediates the apoptosis induction and growth restriction phenotypes of C protein-deficient measles virus. *J. Virol.* **83**, 961–968

39. Itoh, M., Hotta, H., and Homma, M. (1998) Increased induction of apoptosis by a Sendai virus mutant is associated with attenuation of mouse pathogenicity. *J. Virol.* **72**, 2927–2934

40. Koyama, A. H., Irie, H., Kato, A., Nagai, Y., and Adachi, A. (2003) Virus multiplication and induction of apoptosis by Sendai virus: Role of the C proteins. *Microbes Infect* **5**, 373–378

41. Combredet, C., Labrousse, V., Mollet, L., Lorin, C., Delebecque, F., Hurtrel, B., McClure, H., Feinberg, M. B., Brahic, M., and Tangy, F. (2003) A molecularly cloned Schwarz strain of measles virus vaccine induces strong immune responses in macaques and transgenic mice. *J. Virol.* **77**, 11546–11554

42. Calain, P., and Roux, L. (1993) The rule of six, a basic feature for efficient replication of Sendai virus defective interfering RNA. *J. Virol.* **67**, 4822–4830

43. Choi, S. G., Olivet, J., Cassonnet, P., Vidalain, P. O., Luck, K., Lambourne, L., Spirohn, K., Lemmens, I., Dos Santos, M., Demeret, C., Jones, L., Rangarajan, S., Bian, W., Coutant, E. P., Janin, Y. L., *et al* (2019) Maximizing binary interactome mapping with a minimal number of assays. *Nat. Commun.* **10**, 3907

44. Besson, B., Sonthonnax, F., Duchateau, M., Ben Khalifa, Y., Larrous, F., Eun, H., Hourdel, V., Matondo, M., Chamot-Rooke, J., Grailhe, R., and Bourhy, H. (2017) Regulation of NF-kappaB by the p105-ABIN2-TPL2 complex and RelAp43 during rabies virus infection. *PLoS Pathog.* **13**, e1006697

45. Kim, J., and Grailhe, R. (2016) Nanoluciferase signal brightness using furimazine substrates opens bioluminescence resonance energy transfer to widefield microscopy. *Cytometry A* **89**, 742–746

46. Guerbois, M., Moris, A., Combredet, C., Najburg, V., Ruffie, C., Fevrier, M., Cayet, N., Brandler, S., Schwartz, O., and Tangy, F. (2009) Live attenuated measles vaccine expressing HIV-1 Gag virus like particles covered with gp160DeltaV1V2 is strongly immunogenic. *Virology* **388**, 191–203

47. Takeuchi, K., Kadota, S. I., Takeda, M., Miyajima, N., and Nagata, K. (2003) Measles virus V protein blocks interferon (IFN)-alpha/beta but not IFN-gamma signaling by inhibiting STAT1 and STAT2 phosphorylation. *FEBS Lett.* **545**, 177–182

48. Giraudon, P., and Wild, T. F. (1981) Monoclonal antibodies against measles virus. *J. Gen. Virol.* **54**(Pt 2), 325–332

49. Erde, J., Loo, R. R., and Loo, J. A. (2014) Enhanced FASP (eFASP) to increase proteome coverage and sample recovery for quantitative proteomic experiments. *J. Proteome Res.* **13**, 1885–1895

50. Cox, J., and Mann, M. (2008) MaxQuant enables high peptide identification rates, individualized p.p.b.-range mass accuracies and proteome-wide protein quantification. *Nat. Biotechnol.* **26**, 1367–1372

51. Cox, J., Neuhauser, N., Michalski, A., Scheltema, R. A., Olsen, J. V., and Mann, M. (2011) Andromeda: A peptide search engine integrated into the MaxQuant environment. *J. Proteome Res.* **10**, 1794–1805

52. Cox, J., Hein, M. Y., Luber, C. A., Paron, I., Nagaraj, N., and Mann, M. (2014) Accurate proteome-wide label-free quantification by delayed normalization and maximal peptide ratio extraction, termed MaxLFQ. *Mol. Cell Proteomics* **13**, 2513–2526

53. Perez-Riverol, Y., Csordas, A., Bai, J., Bernal-Llinares, M., Hewapathirana, S., Kundu, D. J., Inuganti, A., Griss, J., Mayer, G., Eisenacher, M., Perez, E., Uszkoreit, J., Pfeuffer, J., Sachsenberg, T., Yilmaz, S., *et al.* (2019) The PRIDE database and related tools and resources in 2019: Improving support for quantification data. *Nucleic Acids Res.* **47**, D442–D450

54. Wieczorek, S., Combes, F., Lazar, C., Giai Gianetto, Q., Gatto, L., Dorffer, A., Hesse, A. M., Coute, Y., Ferro, M., Bruley, C., and Burger, T. (2017) DAPAR & ProStaR: Software to perform statistical analyses in quantitative discovery proteomics. *Bioinformatics* **33**, 135–136

55. Smyth, D. J., Cooper, J. D., Bailey, R., Field, S., Burren, O., Smink, L. J., Guja, C., Ionescu-Tirgoviste, C., Widmer, B., Dunger, D. B., Savage, D. A., Walker, N. M., Clayton, D. G., and Todd, J. A. (2006) A genome-wide association study of nonsynonymous SNPs identifies a type 1 diabetes locus in the interferon-induced helicase (IFIH1) region. *Nat. Genet.* **38**, 617–619

56. Ritchie, M. E., Phipson, B., Wu, D., Hu, Y., Law, C. W., Shi, W., and Smyth, G. K. (2015) Limma powers differential expression analyses for RNA-sequencing and microarray studies. *Nucleic Acids Res.* **43**, e47

57. Giai Gianetto, Q., Combes, F., Ramus, C., Bruley, C., Coute, Y., and Burger, T. (2016) Calibration plot for proteomics: A graphical tool to visually check the assumptions underlying FDR control in quantitative experiments. *Proteomics* **16**, 29–32

58. Luck, K., Kim, D. K., Lambourne, L., Spirohn, K., Begg, B. E., Bian, W., Brignall, R., Cafarelli, T., Campos-Laborie, F. J., Charloteaux, B., Choi, D., Cote, A. G., Daley, M., Deimling, S., Desbuleux, A., *et al.* (2020) A reference map of the human binary protein interactome. *Nature* **580**, 402–408

59. Rolland, T., Tasan, M., Charloteaux, B., Pevzner, S. J., Zhong, Q., Sahni, N., Yi, S., Lemmens, I., Fontanillo, C., Mosca, R., Kamburov, A., Ghiassian, S. D., Yang, X., Ghamsari, L., Balcha, D., *et al* (2014) A proteome-scale map of the human interactome network. *Cell* **159**, 1212–1226

60. Rual, J. F., Venkatesan, K., Hao, T., Hirozane-Kishikawa, T., Dricot, A., Li, N., Berriz, G. F., Gibbons, F. D., Dreze, M., Ayivi-Guedehoussou, N., Klitgord, N., Simon, C., Boxem, M., Milstein, S., Rosenberg, J., *et al* (2005) Towards a proteome-scale map of the human protein-protein interaction network. *Nature* **437**, 1173–1178

61. Menche, J., Sharma, A., Kitsak, M., Ghiassian, S. D., Vidal, M., Loscalzo, J., and Barabasi, A. L. (2015) Disease networks. Uncovering disease-disease relationships through the incomplete interactome. *Science* **347**, 1257601

62. Sun, X., Vilar, S., and Tatonetti, N. P. (2013) High-throughput methods for combinatorial drug discovery. *Sci. Transl. Med.* **5**, 205rv1

63. Baum, A., and Garcia-Sastre, A. (2011) Differential recognition of viral RNA by RIG-I. *Virulence* **2**, 166–169

64. Chiang, J. J., Sparrer, K. M. J., van Gent, M., Lassig, C., Huang, T., Osterrieder, N., Hopfner, K. P., and Gack, M. U. (2018) Viral unmasking of cellular 5S rRNA pseudogene transcripts induces RIG-I-mediated immunity. *Nat. Immunol.* **19**, 53–62

65. van der Veen, A. G., Maillard, P. V., Schmidt, J. M., Lee, S. A., Deddouche-Grass, S., Borg, A., Kjaer, S., Snijders, A. P., and Reis, E. S. C. (2018) The RIG-I-like receptor LGP2 inhibits Dicer-dependent processing of long double-stranded RNA and blocks RNA interference in mammalian cells. *EMBO J.* **37**, e97479

66. Zhao, Y., Ye, X., Dunker, W., Song, Y., and Karijolich, J. (2018) RIG-I like receptor sensing of host RNAs facilitates the cell-intrinsic immune response to KSHV infection. *Nat. Commun.* **9**, 4841

67. Jalili, M., Salehzadeh-Yazdi, A., Gupta, S., Wolkenhauer, O., Yaghmaie, M., Resendis-Antonio, O., and Alimoghaddam, K. (2016) Evolution of centrality measurements for the detection of essential proteins in biological networks. *Front. Physiol.* **7**, 375

68. Cheng, F., Kovacs, I. A., and Barabasi, A. L. (2019) Network-based prediction of drug combinations. *Nat. Commun.* **10**, 1197

69. Liberzon, A., Subramanian, A., Pinchback, R., Thorvaldsdottir, H., Tamayo, P., and Mesirov, J. P. (2011) Molecular signatures database (MSigDB) 3.0. *Bioinformatics* **27**, 1739–1740

70. Kelder, T., van Iersel, M. P., Hanspers, K., Kutmon, M., Conklin, B. R., Evelo, C. T., and Pico, A. R. (2012) WikiPathways: Building research

communities on biological pathways. *Nucleic Acids Res.* **40**, D1301–D1307

71. Dixon, A. S., Schwinn, M. K., Hall, M. P., Zimmerman, K., Otto, P., Lubben, T. H., Butler, B. L., Binkowski, B. F., Machleidt, T., Kirkland, T. A., Wood, M. G., Eggers, C. T., Encell, L. P., and Wood, K. V. (2016) NanoLuc complementation reporter optimized for accurate measurement of protein interactions in cells. *ACS Chem. Biol.* **11**, 400–408

72. Bergamaschi, D., Samuels, Y., O'Neil, N. J., Trigiante, G., Crook, T., Hsieh, J. K., O'Connor, D. J., Zhong, S., Campargue, I., Tomlinson, M. L., Kuwabara, P. E., and Lu, X. (2003) iASPP oncoprotein is a key inhibitor of p53 conserved from worm to human. *Nat. Genet.* **33**, 162–167

73. Samuels-Lev, Y., O'Connor, D. J., Bergamaschi, D., Trigiante, G., Hsieh, J. K., Zhong, S., Campargue, I., Naumovski, L., Crook, T., and Lu, X. (2001) ASPP proteins specifically stimulate the apoptotic function of p53. *Mol. Cell* **8**, 781–794

74. Trigiante, G., and Lu, X. (2006) ASPP [corrected] and cancer. *Nat. Rev. Cancer* **6**, 217–226

75. Yang, J. P., Hori, M., Takahashi, N., Kawabe, T., Kato, H., and Okamoto, T. (1999) NF-kappaB subunit p65 binds to 53BP2 and inhibits cell death induced by 53BP2. *Oncogene* **18**, 5177–5186

76. Schuhmann, K. M., Pfaller, C. K., and Conzelmann, K. K. (2011) The measles virus V protein binds to p65 (RelA) to suppress NF-kappaB activity. *J. Virol.* **85**, 3162–3171